LIQUID CRYSTAL-BASED BIOSENSORS FOR THE DETECTION OF BILE ACIDS

by

SIHUI HE
B.S. Zhejiang University, 2009
M.S. University of Central Florida, 2011

A dissertation submitted in partial fulfillment of the requirements
for the degree of Doctor of Philosophy
in the College of Optics & Photonics
at the University of Central Florida
Orlando, Florida

Summer Term
2015

Major Professors: Jiyu Fang, Shin-Tson Wu

ABSTRACT

Bile acids are physiologically important metabolites, which are synthesized in liver as the end products of cholesterol metabolism and then secreted into intestine. They are amphiphilic molecules which play a critical role in the digestion and absorption of fats and fat-soluble vitamins through emulsification. The concentration of bile acids is an indicator for liver function. Individual suffering from liver diseases has a sharp increase in bile acid concentrations. Hence, the concentration level of bile acids has long been used as a biomarker for the early diagnosis of intestinal and liver diseases.

Conventional methods of bile acid detection such as chromatography-mass spectrometry and enzymatic reactions are complex and expensive. It is highly desired to have a simple, fast, and low-cost detection of bile acids that is available for self-testing or point-of-care testing. To achieve this goal, we develop a liquid crystal-based biosensor for the detection of bile acids. The sensor platform is based on the anchoring transition of liquid crystals (LCs) at the sodium dodecyl sulfate (SDS)-laden LC/aqueous interface for the detection of bile acids in aqueous solution. The first part of this dissertation focuses on the detection mechanism of bile acids. Our studies show that the displacement of SDS from the LC/aqueous interface by the competitive adsorption of bile acids induces a homeotropic-to-planar anchoring transition of the LC at the interface, providing an optical signature for the simple and rapid detection of bile acids. The adsorption of bile acids on the interface was found to follow Langmuir-Freundlich isotherm. The adsorption kinetics of different bile acids is compared. We find that both the number and position

of hydroxyl groups of bile acids affect their adsorption kinetics. The different optical patterns of LC films formed by the adsorption of bile acids are also discussed.

The second part of this dissertation studies the effect of solution conditions, surfactants, and liquid crystals on the detection limit of the LC-based biosensor for bile acids. Low pH and high ionic strength in the aqueous solution can reduce the electrostatic interaction between SDS and bile acids, which leads to a decreased detection limit. Surfactants with smaller headgroup and lower packing density also help to reduce the detection limit. To further reduce the detection limit, we investigate the effect of LC structures and find that LCs with a shorter chain length give lower detection limits. Also, by substituting a phenyl ring with a cyclohexane ring, we find that the detection limit is further reduced due to the decrease of the interaction between the phenyl rings of LCs. By mixing different LCs together, the detection limit can be linearly tuned from 160 μM to 1.5 μM, which is comparable to the traditional methods. But the LC-based biosensors have much simpler design and manufacture process.

The third part of this dissertation is to apply this LC-based biosensor to the detection of urinary bile acids. We test the influence of several potential interfering species such as urea, creatinine, uric acid and ascorbic acid by conducting experiments in synthetic urine. By adjusting the concentration of SDS, we are able to eliminate the impact of those interfering species, and demonstrate that the LC-based biosensors can selectively detect urinary bile acids in human urine, suggesting its potential for screening liver dysfunctions.

The final part of this dissertation is to investigate the application of LC-based biosensors in detecting the lipolysis process by porcine pancreatic lipase (PPL). It has been a long-standing argument over the role of bile salts on the activity of PPL. Thus, we study the time course of the

hydrolysis of phospholipid L-dipalmitoylphosphatidylcholine (L-DPPC) by PPL at LC/aqueous interface. The hydrolysis of L-DPPC leads to a homeotropic-to-tilted anchoring transition of the LC at the interface, which allows the hydrolysis process to be monitored by a polarizing optical microscope. The microscopy image analysis reveals a lag-burst kinetics where a lag phase is followed by a burst phase. The effect of bile acids on these two phases is studied. We find that the activity of PPL both in the presence and absence of colipase can be improved by increasing the concentration of bile acids. The improvement becomes more distinct in the presence of colipase.

ACKNOWLEDGMENTS

As I am close to the end of my tortuous journey of Ph. D. program, I really want to appreciate so many people that have been assisting, encouraging, and companying me in each part of the journey.

First, I would like to take this opportunity to express my most sincere gratitude and appreciation to my Ph. D advisor Dr. Shin-Tson Wu and co-advisor Dr. Jiyu Fang for their help, support and valuable discussions throughout my research. Dr. Wu provides the direction and vision of my research to a practical application. Dr. Fang guides me through each step to obtain a better understanding of my research. It has been my great luck and honor being their students. I like that they shared stories with me, always pointed out my mistakes or shortcomings to help me improve, and encouraged me when I was frustrated. Their constant guidance and persistent spirit helped me substantially in the research work.

I am grateful to Dr. Pieter G. Kik and Dr. Stephen Kuebler for serving on my thesis committee and for their encouragement and insightful comments.

I also appreciate Dr. David Hagan and Dr. Eric Van Stryland for their guidance during my first two years of Ph. D. pursuit. They helped me learn the importance of independent study.

Besides, I like to thank my colleagues in Microsoft Applied Sciences Group during my internship. They gave me a chance to apply what I've learnt at UCF to build a lab and achieve the goals in my internship project there. What I've leant there enlightened me to move further on my Ph. D. project.

I am very grateful for all my colleagues and friends at UCF, especially my lab mates Dr. Wenlang Liang, Jinan Deng, and Dr. Tanmay Bera in Dr. Fang's group and Dr. Jie Sun, Fenglin Peng in Dr. Wu's group. They gave me a lot of help both in research and life.

I am also very thankful to our financial support from Industrial Technology Research Institute (ITRI) in Taiwan.

Last, I want to give special thanks to my parents. Even though they are far away from me, their selfless love and support always give me strength to chase my dreams.

TABLE OF CONTENTS

LIST OF FIGURES

LIST OF TABLES

CHAPTER 1 INTRODUCTION

1.1 Bile Acids

Bile acids are water-soluble, biological surfactants found predominantly in bile [1]. The term "bile acid" was named to describe the acidic components in bile, which has been studied since as early as 1807 [2]. Because of their important functions unique physical properties, bile acids have attracted attentions from both scientists and clinicians for centuries. Bile acids play major roles in the cholesterol metabolism in liver, the stimulation of bile flow and binary phospholipid secretion in bile, and the lipid digestion in intestine [3]. They are synthesized from the conversion of cholesterol by liver. Bile acids have a large, rigid and quasi-planar steroid ring system composed of four rings, where three of them are cyclohexane and one is cyclopentane (Figure 1). This steroid ring system serves as the skeleton of the bile acids with a banana shape. There are methyl groups and hydrogen atoms at the convex face and hydroxyl groups at the concave face. Hence, the convex side is hydrophobic and the concave side is hydrophilic. All bile acids have a hydroxyl group at C-3 position (denoted in Figure 1), which is derived from cholesterol. Bile acids differ from the number and positions (R_1 and R_2) of the hydroxyl group (Table 1). The direct products of the cholesterol metabolism are called primary bile acids, which include cholic acid (CA) and chenodeoxycholic acid (CDCA). They are conjugated with glycine or taurine by hepatocytes to enhance their hydrophilicity before secreted to gallbladder, which stores bile during the interdigestive phase [4]. Upon meal digestion, bile acids are discharged into duodenum by gallbladder contraction to digest lipids and lipid-soluble vitamins. In the distal small intestine (ileum) and colon, bile acids are deconjugated and dehydroxylated by bacterial enzymes[5-7]. This gives the secondary bile acids including deoxycholic acid (DCA) and

lithocholic acid (LCA), which are dehydroxylated from CA and DCA, respectively. Around 95% of total bile acids are reabsorbed and transported back to liver through portal venous circulation, where conjugated bile acids are formed and secreted to gallbladder again[8]. This continuous cycle of absorption and secretion between liver, gallbladder, and intestine is termed the enterohepatic circulation.

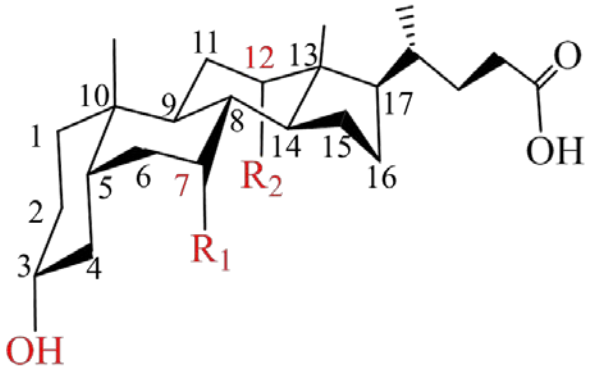

Figure 1: Structure of bile acids with the atom numbering of the steroid skeleton

Table 1 Types of bile acids

Categories	**Bile acids**	**R_1**	**R_2**
Primary	Cholic acid (CA)	OH	OH
	Chenodeoxycholic acid (CDCA)	OH	H
Secondary	Deoxycholic acid (DCA)	H	OH
	Lithocholic acid (LCA)	H	H

1.1.1 Bile Acids in Lipid Digestion

Lipid hydrolysis (lipolysis) of triglyceride is mainly performed by three lipases: lingual, gastric, and pancreatic lipase, which occur in mouth, stomach, and duodenum, respectively [9]. Lingual and gastric lipases hydrolyze triglycerides into fatty acids and diglycerides. These lipolysis products are polar lipids, which often accumulate at the lipid/aqueous interface, resulting in the inhibition of further lipolysis [10]. Therefore, only 30% of dietary lipids can be hydrolyzed by lingual and gastric lipases.

During lipid digestion in duodenum, bile acids are released to duodenum by gallbladder contraction. As bile acids are highly surface active [11], they can competitively adsorb at protein or polar lipid-laden lipid/aqueous interface, and displace the protein or polar lipids from the interface [12, 13]. The displacement disrupts the packing of protein or polar lipids at the interface, hence facilitates the access of lipolytic enzymes to dietary lipids. Besides, bile acids also form mixed micelles with lipids, which improves the uptake of lipids in intestine [14].

1.1.2 Bile Acids as Biomarkers for Liver Diseases

During the enterohepatic circulation, the efficiency of extracting bile acids from portal vein to the liver by the hepatocytes is very high (75 – 90% first-pass clearance). Therefore, the concentration of bile acids in peripheral blood is very low (less than 10 μM) compared to the portal concentration of bile acids (60 – 80 μM) [15, 16]. For people with liver dysfunction, the extraction efficiency of bile acids decreases, which leads to high concentration of bile acids in serum and urine. Therefore, bile acids have long been used as a biomarker for liver diseases.

The detection of bile acids can be dated back to 1844 when M. Von Pettenkofer demonstrated the color reaction between cholic acid and sugar in sulfuric acid [17]. Over a hundred

years, this reaction has been modified in numerous ways until the introduction of chromatographic methods. Various chromatography technologies including gas chromatography and high-performance liquid chromatography (HPLC) are commonly used in combination with mass spectrometry to detect bile acids [17-19]. The major drawback of gas chromatography is the need for volatility, which requires the cleavage of conjugated bile acids and derivatisation [17, 20]. This drawback was eliminated by HPLC. Currently, with HPLC-electrospray tandem mass spectrometry (MS), the detection limit for bile acids can be as low as 1 nM[19]. It can also distinguish bile acids with different number and positions of hydroxyl groups. The high sensitivity and selectivity of HPLC-MS makes it a great analytical method for the detection of bile acids. However, the sample preparation and analysis of the HPLC-MS method are very complex. The sample preparation includes extraction of bile acids from the sample matrix and the separation of bile acids. A lot of studies have been involved in solvent and polymers for the sample preparation [21-23].

Enzymatic reactions are a simple method for the detection of bile acids [24-26]. Figure 2 shows the principle of the method. Bile acid molecules with 3α-hydroxysteroid are repeatedly oxidized and reduced by enzyme 3α-hydroxysteroid dehydrogenase (3α-HSD) in the presence of co-enzyme thio-NAD^+ and NADH, which accumulate reduction product thio-NADH and oxidation product NAD^+, respectively. Thio-NADH has an absorption peak at 405 nm, which can be characterized by UV-Vis spectroscopy. The ratio of thio-NADH formation is proportional to the concentration of bile acids, and thereby the concentration of bile acids can be determined. This cycling method enables significant signal amplification, giving a detection limit of 0.5 μM. The enzymatic reactions were also characterized with electrochemical measurements. For

example, S. Koide et al. immobilized three enzymes on a sensor chip and detected the electrode reaction of the product of enzymatic reaction [26]. They showed that the detection limit for bile acids could reach 2 μM. Compared to chromatography, enzymatic reactions are simple and have been widely used for clinical detection of bile acids. A drawback of this method involves multiple enzymatic reactions and expensive enzymes. In addition, Bile acids are measured indirectly from the product of Thio-NADH, therefore the result is highly dependent on the purity of the enzyme. Furthermore, this enzymatic reaction relies on the 3α-hydroxy group of bile acids. For patients with HSD3B7-deficiency, they have bile acids with a 3β-hydroxy group, which can escape from the detection of bile acids, leading to misjudgment.

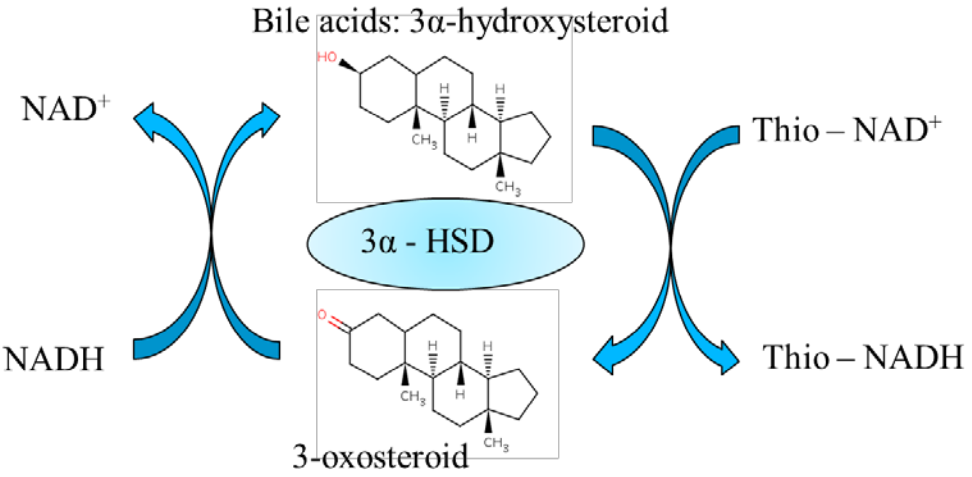

Figure 2: Principle of enzymatic cycling methods for the detection of bile acids.

Recently, other methods for detecting bile acids are also investigated [27, 28]. For example, Y. Liu et al. synthesized β-cyclodextrin (β-CD) derivatives with fluorophores. The binding ability of β-CD derivatives with bile acids can be monitored by observing the fluorescence intensity change of the fluorophores [27]. Z. Wu et al. fabricated 3D ordered macroporous hydrogels with nanocavities derived from the molecular imprinting of bile acids. The 3D ordered

macroporous hydrogels show the reflection band of incident light, while the nanocavities allow the recognition of the bile acids. When the targeted bile acid adsorbs to the binding sites of the nanocavities, the period of the hydrogel changes, which leads to a shift of reflection wavelength. The detection limit of this method for bile acids can be as low as 1pM. However, this method requires complex fabrication process of 3D ordered macroporous hydrogels [28]. Therefore, it is highly desired to develop a simple and fast method to detect bile acid with sufficient sensitivities.

1.2 Liquid Crystals

Liquid crystals (LCs) are an intermediate phase between liquid phase and crystalline phase. In a liquid phase, molecules don't have any order, while in a crystalline phase, molecules have both positional and orientational order. In a LC phase, molecules have long-range orientational order and sometimes some positional order. Because of the remaining order, LCs exhibit optical and dielectric anisotropies. The energy required to change the order remained in LCs is very small, which make them unique soft materials for displays, photonic and biomedical applications.

LCs are generally catalogued to two classes: thermotropic LCs and lyotropic LCs. Thermotropic LCs can be single compound, whose phase transition is driven by thermal processes. Lyotropic LCs are composed of at least two compounds, usually amphiphilic molecules and solvent. The phase transition of lyotropic LCs depend on the concentration of components. Lyotropic LCs are often found in biological systems. Compared to thermotropic LCs, lyotropic LCs have a relatively small birefringence and dielectric anisotropy. Therefore, thermotropic LCs are more sensitive to external stimuli, and hence being extensively studied and widely applied to different fields. In this dissertation we will focus on thermotropic LCs.

The shapes of thermotropic LC molecules can be rod-like (calamitic), disk-like (discotic), bowlic, or banana. The rod-like LCs are widely used because they have high birefringence and large dielectric anisotropy. Achiral rod-like LCs exhibit smectic and/or nematic phases. In a smectic phase, LC molecules possess positional order in one direction and orientational order. In a nematic phase, LC molecules only have orientational order, which makes them easy to be aligned by an external force. Therefore, we will apply the nematic LC in our sensor platforms.

1.2.1 Orientational Order of Nematic Liquid Crystals

The average orientation of LCs is referred as the director $\vec{n}$, which is the direction where most of the long axis of LC molecules pointing to, as shown in Figure 3.

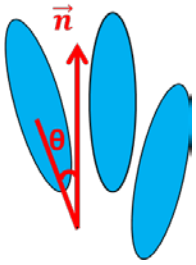

Figure 3: Director $\vec{n}$, and the angle θ which denotes the deviation of the long axis of a molecule from director.

The ordering in nematic LCs can be described by order parameter S, which is defined as,

$$\boldsymbol{S = \frac{1}{2}(3\langle cos^2\theta\rangle - 1)}$$

For an isotropic liquid, S = 0; for an ideal crystal, S = 1; and for a nematic LC, S ~ 0.3 – 0.4 near the nematic-isotropic transition, and S ~ 0.6 – 0.8 in the nematic phase [29]. The orientation of nematic LCs is determined by the minimization of free energy. The total free

energy of LC films can be written as a function of their elastic energy, surface anchoring, and external forces [30],

$$F = F_{Homogeneous} + F_{Field} + F_{Elastic} + F_{Surface} \quad (1)$$

where $F_{Homogeneous}$ is the homogeneous free energy, which is the internal energy of homogeneous nematic LCs, expressed in terms of an expansion in the order parameter S [31],

$$\boldsymbol{F_{Homogeneous} = f_0 + \frac{1}{2}a(T - T^*)S - \frac{1}{3}bS^3 + \frac{1}{4}cS^4} \quad (2)$$

where a, b, c > 0 and are temperature independent. T* is the supercooling temperature limit of the bulk liquid phase.

$$\boldsymbol{F_{Field} = -\frac{1}{2}\varepsilon_0\Delta\varepsilon\left[\vec{E}\cdot\vec{n}\right]^2 - \frac{1}{2}\frac{\Delta\chi}{\mu_0}\left[\vec{B}\cdot\vec{n}\right]^2} \quad (3)$$

where F_{Field} is the free energy due to electric and magnetic fields. ε_0, $\Delta\varepsilon$, and $\vec{E}$, are electric permittivity of vacuum, dielectric anisotropy and electric field vector, respectively; χ_0, $\Delta\chi$, and $\vec{B}$ are permeability of vacuum, diamagnetic anisotropies, and magnetic field vector, respectively.

$$\boldsymbol{F_{Elastic} = \frac{1}{2}K_{11}(\nabla\cdot\vec{n})^2 + \frac{1}{2}K_{22}(\vec{n}\cdot\nabla\times\vec{n})^2 + \frac{1}{2}K_{33}(\vec{n}\times\nabla\times\vec{n})^2} \quad (4)$$

where $F_{Elastic}$ is the elastic energy density of bulk LCs under three basic deformations: splay, twist, and bend; K_{11}, K_{22}, and K_{33} are splay, twist, and bend elastic constants, respectively. $K_{ii} \sim 10^{-11}$ N for typical nematic LCs. The elastic energy stored in bulk LCs indicates the long-range orientational order of LCs. Because of this weak elastic constant, the LC orientation is very sensitive to external stimuli given by electric field, magnetic field, or surface anchoring. This allows for the wide applications of liquid crystals in display, sensing, and other photonic devices.

$$\boldsymbol{F_{Surface} = \gamma_{iso} + \gamma_g + \gamma_{aniso}} \quad (5)$$

where $F_{Surface}$ is interfacial free energy. $\boldsymbol{\gamma_{iso}}$ is orientational independent, which is called interfacial tension for isotropic interfaces; $\boldsymbol{\gamma_g}$ is the gradient interfacial free energy, which is a function of saddle-splay elastic constant K_{24} and second order splay-bend elastic constant K_{13}; $\boldsymbol{\gamma_{aniso}}$ is the free energy from the surface anchoring or bulk distortions that make the director deviated from its preferred orientation in the absence of perturbations. The preferred orientation of the LC director is called "easy axis". For the case of weak anchoring, $\boldsymbol{\gamma_{aniso}}$ can be written in terms of the polar and azimuthal angles (ϕ_p and ϕ_a, respectively) of the LC director from the easy axis,

$$\boldsymbol{\gamma_{aniso} = \frac{1}{2} W_p sin^2 \phi_p + \frac{1}{2} W_a sin^2 \phi_a} \quad (6)$$

where W_p and W_a are the polar and azimuthal anchoring energies. The typical values for W_p are 1 – 1000 μJ/m^2 [32]. In a micrometer thick LC layer, this anchoring energy is in the same order of the bulk elastic energy. This makes it possible for a micrometer-thick LC film to respond to surface perturbation.

1.2.2 Biomedical Applications of Liquid Crystals

In biomedical imaging systems, LCs have been used as a tunable filter or a spatial light modulator to screen cells and tissues in innovative ways[33, 34]. This tunable ability of LCs comes from their electro-optic properties indicated by Equation (3). The applied electric or magnetic fields can change the orientation of LC molecules, and hence the refractive index of LC layers, leading to the phase and retardation change of light passing through the LC layer. When placed between two crossed polarizers, the amplitude of light can be modulated. Therefore, the information carried within the phase or amplitude of light can be filtered or modified.

LCs can also be applied to tunable laser sources for probing or imaging biomedical systems by changing the band gap of periodic LC structures through their electro-optic properties [35]. Besides, electrically tunable LC adaptive lenses are also developed [36, 37]. They hold promise to correct near and far vision for old people with presbyopia.

Beyond the electro-optic properties of LCs, the interface properties of LCs have also been investigated. As indicated by equations (5) and (6), the orientation of LCs is related to the surface anchoring. The changes of the surface in contact with LCs often lead to the change in the surface anchoring. Due to the elastic nature of LCs, the surface induced ordering of LCs can extend to tens of micrometers into bulk LCs [38], which magnifies the molecular events at LC surface. Because of the birefringence of LCs, the change of their orientations can be visualized under crossed polarizers. Therefore, LCs can serve as an optical amplification probe for molecular events at the LC surface.

A lot of studies have been done on the anchoring of LCs at the LC/solid interface [39-41]. A well-studied solid surface is a mechanically rubbed polyimide layer, which anchors the LC by van der Waals dispersion forces [42]. The anchoring energy by rubbed polyimide layer is ~ 300 $\mu J/m^2$ (surface anchoring ~100 $\mu J/m^2$ is considered as strong, and ~ 1 $\mu J/m^2$ is considered as weak)[42, 43], therefore, the tilt angle of the LC at the LC/solid interface is determined by the polyimide layer. There are some other studies that use LC to visualize the self-assembly of molecules [40, 44-46]. For example, Gupta et al. showed different azimuthal orientations of LCs by the self-assembled monolayers (SAM) of alkanethiols with odd and even chain lengths formed on obliquely deposited films of gold [40]. The odd-even modulation of LC orientations was hypothesized to be due to the change of the methyl orientation of alkanethiols, which led to a

change in the dielectric properties of SAM, and further led to a change in the LC orientation due to the flexoelectric polarization effect (deformation-induced polarization) of LC. Fang et al. applied LCs to observe the organization of molecular tilt azimuth of surfactant monolayers, which could only be observed by lateral force microscopy previously [45]. Cheng et al. imaged micropatterned SAM with LCs, which showed the spatial resolution of at least 4 μm [46].

The LC/aqueous interface has attracted more attention in the past decade because it gives certain mobility of molecules to change the orientation of LCs [42], which allows the investigation of molecular interactions at the LC/aqueous interface. There are two major platforms to study the molecular interactions at LC/aqueous interfaces. One is the spherical interfaces of LC droplets in an emulsion, the other is the planar interfaces formed by confining LC films within transmission electron microscopy (TEM) grids.

In the LC droplet platform, the LC droplets dispersed in aqueous solution are usually stabilized by surfactants or polymers. The orientational order of the LC droplets is determined by the balance of the surface anchoring and the elastic energy, whereas the elastic energy depends on the size of LC droplets. To make monodispersed LC droplets, Gupta et al. synthesize polymeric multilayer “shells” for the encapsulation of LC droplets [47]. With this monodispersed LC droplet system, they studied the oreintational order of the encapsulated LC droplets in response to the adsorption of sodium dodecyl sulfate (SDS) [48]. Figure 4 shows the orientational change of the LC droplet (top row), which can be determined from the optical appearance of LC droplet under a bright field (middle row) and polarized light microscope (bottom row). Without SDS, the LC adopts a tangential alignment at the LC/aqueous interface. As the concentration of

SDS increases, the LC becomes tilted at the interface, and eventually aligns perpendicular at the interface.

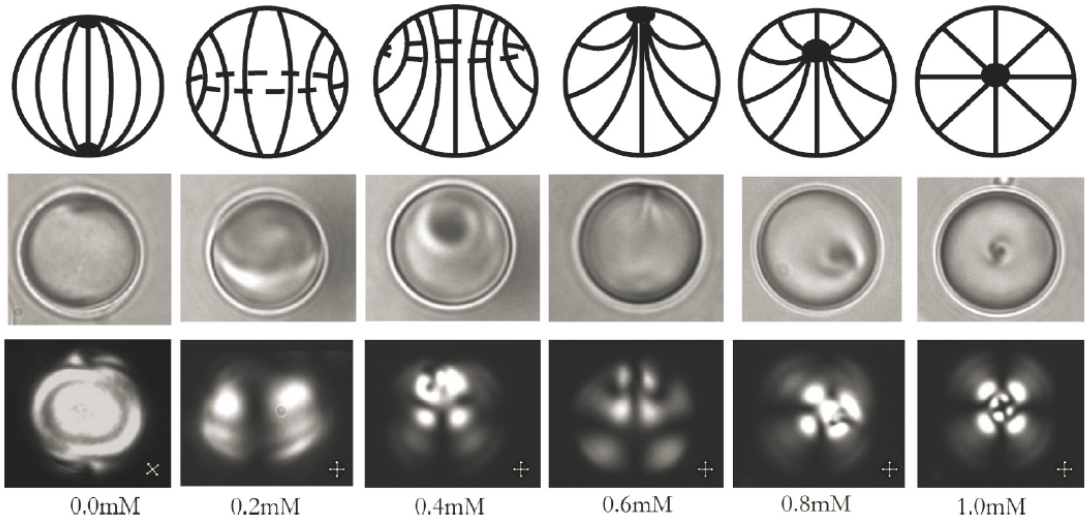

Figure 4: Surface-driven ordering transitions within LC droplets of fixed size. The change in the surface anchoring of the LC droplet (from tangential to perpendicular) was achieved by equilibrating 8.0 (0.2- μ m-diameter, polymer-encapsulated liquid crystal 5CB droplets with aqueous solution containing surfactant SDS at concentrations from 0 to1mM. The top row shows the schematic illustration of the topological ordering of the LC within each droplet. The middle and bottom rows show the corresponding bright-field and polarized light micrographs of the 5CB droplets, respectively. Adapted from Gupta, J. K.; Zimmerman, J. S.; de Pablo, J. J.; Caruso, F.; Abbott, N. L. Langmuir 2009, 25, 9016-9024 (copyright 2009 American Chemical Society)

LC droplets dispersed in aqueous solution are remarkably sensitive to endotoxin. For example, Lin et al. reported the orientational transition of LC triggered by extremely low concentrations of endotoxin (< 1 pg/mL) [49]. This high sensitivity is explained to be the result of

the adsorption of endotoxin at the defects of the LC droplets. The interaction between the endotoxin and LC defect changes the orientation of the LC droplets. Despite the high sensitivity of the LC droplet platforms, the synthesis of monodispersed LC droplets still remains a difficult task.

The platform of a planar nematic LC/aqueous interface for the study of molecular interactions was initiated by Nicholas's group [50]. Figure 5 shows the setup used to generate the planar LC/aqueous interface, in which a LC film is confined in a metallic grid placed on a functionalized solid substrate. The thickness of the confined LC film is approximately the same as the thickness of the metallic grid [51]. This setup is then immersed in aqueous solution, which forms a planar LC/aqueous interface. With this setup, the molecular interaction at the planar LC/aqueous interfaces can be easily visualized.

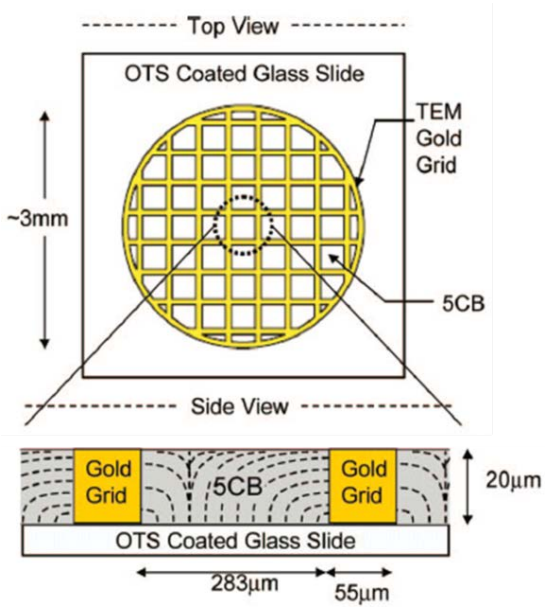

Figure 5: Schematic illustration of the experimental geometry used to prepare the interface between an aqueous phases and an immiscible thermotropic LC phase. Adapted from Gupta, J. K.; Tjipto, E.; Zelikin, A. N.; Caruso, F.; Abbott, N. L. Langmuir 2008, 24, 5534-5542 (copyright 2008 American Chemical Society).

Brakes et al. used the confined LC film to report the binding and enzymatic reaction of phospholipase A_2 at phospholipid-laden LC/aqueous interface [52]. Phospholipid monolayers at the LC/aqueous interface caused homeotropic alignment of LCs. Different interactions (binding or enzymatic reaction) between phospholipase A_2 and phospholipids (D-DPPC, L-DLPC, and L-DPPC) can be visualized at the LC/aqueous interface. The binding of phospholipase A_2 to the phospholipids D-DPPC at the interface (without enzymatic reaction) led to tilted or planar orientations of LCs. The enzymatic reaction between phospholipase A_2 and phospholipids L-DLPC or L-DPPC led to the formation of different domains at the LC/aqueous interface. Tan et al. designed the LC/aqueous interface for the detection of ligand-receptor interaction [53].

Specifically, they found that the avidin-functionalized LC/aqueous interface would capture the biotin-functionalized vesicles, leading to the planar-to-homeotropic anchoring transition of LCs. Price et al. reported the orientational transition of the LCs from at the LC/aqueous interface from tilted alignment to homeotropic alignment triggered by DNA hybridization [54]. The LC/aqueous interface was decorated by single-stranded DNA (ssDNA)/surfactant octadecyltrimethylammonium bromide (OTAB) complex, and the LC at the interface assumes a tilted orientation. The exposure of the ssDNA/OTAB laden LC/aqueous interface to its ssDNA complement led to the hybridization of the two ssDNA into double-stranded DNA, resulting in the condensation of dsDNA/OTAB at the interface, which triggered the orientational transition of LCs from tilted alignment to homeotropic alignment. Hu et al. imaged the molecular interactions between cationic antimicrobial peptides and negatively charged lipids at the LC/aqueous interface [55]. The electrostatic interaction at LC/aqueous interface disrupted the packing of the lipids at the interface, leading to homeotropic-to-planar transition of the LC at the interface.

In this dissertation, we design a sensor platform based on the anchoring transition of the LC at the SDS-laden LC/aqueous interface for the detection of bile acids in aqueous solution. We study the detection mechanism of the sensor platform and its detection limit for bile acids. Finally, we demonstrate the potential application of the sensor platform for the detection of urinary bile acids and the effect of bile acids in lipolysis processes.

1.3 Conclusion

Bile acids are amphiphilic molecules which play an important role for the digestion of fat and fat-soluble vitamins. As bile acids are regulated by liver, they are an important biomarker for the diagnosis of liver dysfunction in early stage. The increase of bile acid concentration is a sign of liver dysfunction. The current methods for the detection of bile acids are complex and require special techniques. Therefore, we aim to develop a LC-based sensor platform for the simple and fast detection of bile acids with the goal of screening liver disease.

CHAPTER 2 DETECTION MECHANISM

2.1 Formation of Surfactant-Laden LC/Aqueous Interfaces

The experimental setup of the LC-based biosensor is shown in Figure 6, in which a polyimide-coated glass substrate was used to induce the perpendicular alignment of LCs. A TEM grid (18 μm thickness, 285 μm grid spacing, and 55 μm bar width) is placed on polyimide-coated glass substrates. One microliter of LC was filled in the pores of the TEM grids supported by the polyimide-coated glass substrates. The excess LC was removed by using a capillary tube, leading to the formation of LC films in the pores of the grids. The system was then immersed in aqueous solution containing SDS. The adsorption of SDS leads to the formation of a surfactant-laden LC/aqueous interface.

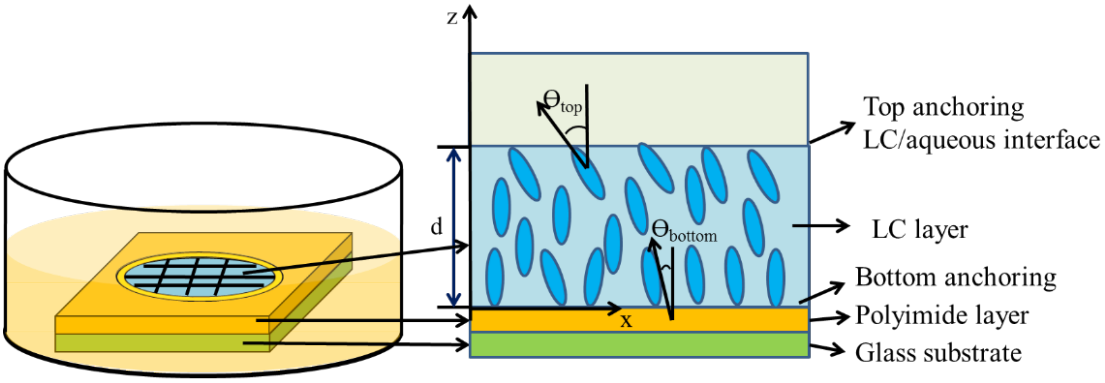

Figure 6: Schematic illustration of the experimental setup for the LC-based biosensor.

The LC we use in this section is 4-cyano-4'-pentylbiphenyl (5CB). It is a room-temperature nematic LC. The chemical structure of 5CB is shown in Figure 7.

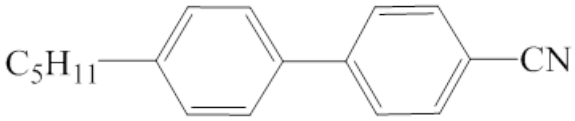

Figure 7: Chemical structure of 5CB

The TEM grid can prevent the dewetting of LCs on the glass substrate [50]. It is found that sharp edges can cause the hysteresis of contact angle and inhibit the move of contact line of liquids on a solid surface [56]. Similarly, a TEM grid can pin the contact line of LCs and confine them in the pores. The pore size of TEM grids is also important. If the pore size is large, LCs may not be confined well to form a flat film in the grids. If the pore size is small, the anchoring of LCs by the grid can dominate the orientation of LCs. It has been found that the TEM grid with 285 μm is suitable for this system [50].

The parameter charactering anchoring strength is the extrapolation length, given by L = K/W, where K is the elastic constant of LCs, and W is the anchoring energy per unit area. The extrapolation length is the distance from the real surface to an extrapolated surface where LC director aligns in the direction of easy axis. For strong anchoring, L << thickness of LC film (d). For 5CB, the average elastic constant K ~ 6 pN [57, 58]. The anchoring energy by polyimide is typically ~ 300 μJ/m^2 [42, 43]. So the extrapolation length is estimated to be 20nm, which is much smaller than the thickness of the LC film confined in the TEM grid (18 μm). Therefore, the bottom anchoring of the LC is very strong, which leads to the perpendicular alignment of LC ($\Theta_{bottom} = 0^o$ in Figure 6).

The top anchoring of the LC depends on the density of the surfactant tail at the LC/aqueous interface [59], which in turn is related to the concentration of SDS and the ionic strength in the aqueous phase. In deionized water, LCs assume planar alignment ($\Theta_{top} = 90^o$) at

the interface. As the concentration of SDS increases in the aqueous phase, the tilt angle decreases (Figure 8a, b, c). When the concentration of SDS reaches to a critical value, LCs assume vertical alignment which shows dark appearance under crossed polarizers (Figure 8c,d). It has been shown that the critical concentration of SDS required to induce the vertical alignment of LC at the interface is 1.8 mM [60]. The density of the SDS at the interface can be approximated by making an analogy of the adsorption of SDS at LC/aqueous interface to the adsorption of SDS at air/water interface [59, 61]. It has been shown that the molecular area of SDS at the air/water interface is about 63 $Å^2$/molecule with bulk concentration of 1.8 mM [62].

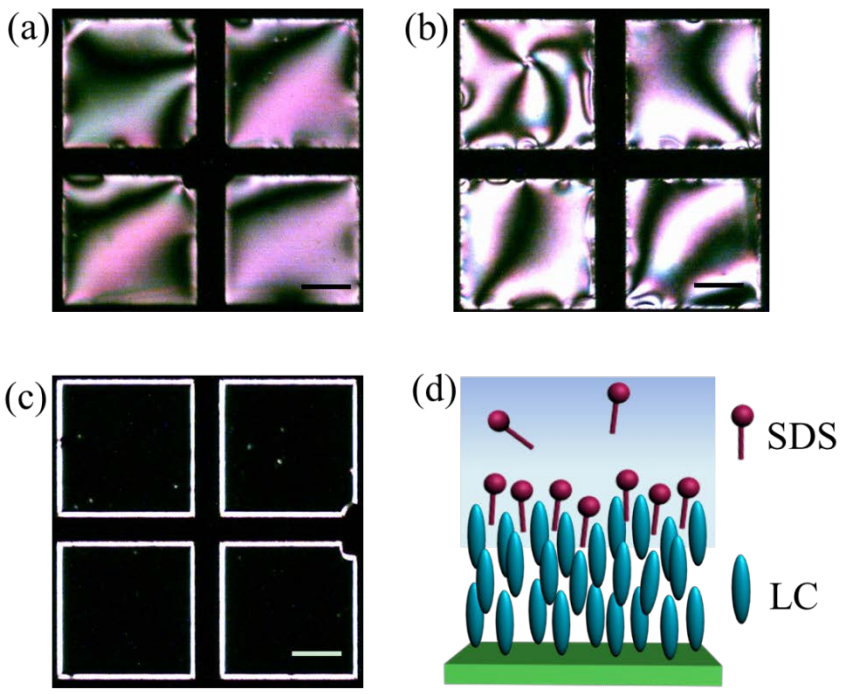

Figure 8: Polarizing optical microscopy images (a, b,c) and schematic illustration (d) of LC films in water without (a) and with SDS of 1.4 mM (b) and 1.8 mM (c, d). The LC here is 5CB. Scale bar: 97 µm.

In phosphate buffered saline (PBS) solution, the high ionic strength (172 mM) can improve the adsorption constant of SDS. It has been found that the adsorption constant in Langmuir isotherm of SDS can increase by two orders in 100 mM sodium chloride solution [63]. Therefore, only 50 µM SDS in PBS solution can induce the homeotropic alignment of the LC at the interface.

2.2 Mechanism for the Detection of Bile Acids

Cholic acid (CA) is one of the two primary bile acids synthesized by liver. When CA is added into the aqueous phase side of the SDS-laden LC/aqueous interface, we find that the optical appearance of the LC films in the pores of TEM grids changes from a dark appearance to

bright domains (Figure 9a). The appearance of the bright domains reflects a continuous change in the orientation of the LC from a homeotropic anchoring at the polyimide-coated glass substrate to a planar anchoring at the SDS-laden LC/aqueous interface [52].

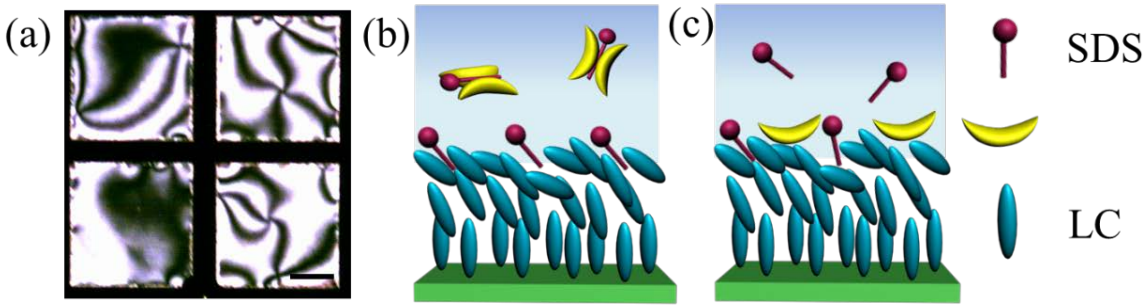

Figure 9: Polarizing optical microscopy images (a) and schematic illustrations (b, c) of the SDS-laden LC/aqueous interface after being exposed to 30 μM CA solution for 12 hours. The LC here is 5CB. Scale bar: 97 μm.

There are two possible mechanisms that lead to the anchoring transition of the LC at the SDS-laden LC/aqueous interface. One is that CA can form micelles with the SDS in the aqueous phase (Figure 9b). The micelle formation may change the adsorption isotherm of SDS at the LC/aqueous interface, leading to the decrease of SDS density at the interface. This decrease of SDS interfacial density could lead to large tilt angle of LC. Another possible mechanism is that CA can competitively adsorb at the LC/aqueous interface and displaces the SDS from the interface, lie flat at the oil/aqueous interface [64], and lead to the anchoring transition of the LC at the interface (Figure 9c). To verify the possible mechanisms, we conducted the controlled experiment with fluorescence-labeled CA (CLF, Figure 10a). For the first possible mechanism, we expect to see the anchoring transition of the LC without fluorescence from the LC/aqueous interface. For the second mechanism, we expect to see the anchoring transition of the LC with

fluorescence at the LC/aqueous interface. Our experiment shows that even at a very low concentration of CLF which cannot trigger the anchoring transition of the LC at the interface, the fluorescence at the interface has already been observed (Figure 10b,c). This confirms the second mechanism: the anchoring transition of the LC at the interface is due to the competitive adsorption of CA. This mechanism is consistent with the function of bile acids in intestine, where they competitively adsorb onto the lipid interface of gastric emulsions and disrupt the packing of the lipids.

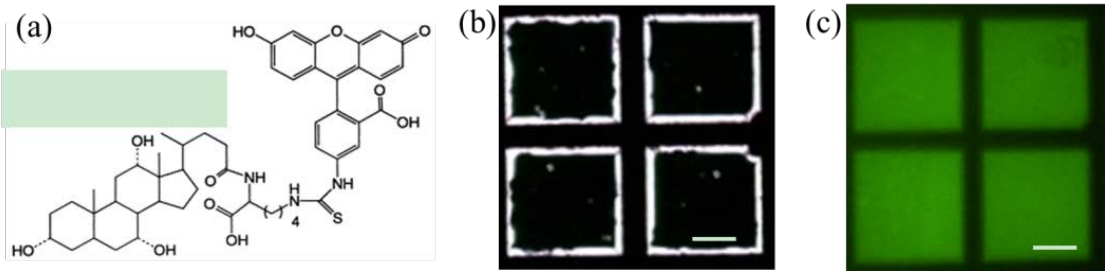

Figure 10: The chemical structure of CLF (a), polarizing (b) and fluorescence (c) microscopy images of a SDS-laden LC/aqueous interface after being exposed to 0.02μM CLF solution. The LC here is 5CB. Scale bar: 97 μm.

Figure 11 shows the fluorescence intensity at different CLF concentrations. The fluorescence intensity is measured by a fluorescent microscope. It reflects the adsorption of CLF at the SDS-laden LC/aqueous interface, which can be fitted well by Langmuir-Freundlich isotherm with $R^2 = 0.997$. The Langmuir-Freundlich isotherm is given by [65],

$$\mathbf{q}_e = \frac{\mathbf{q}_{max}(KC_e)^n}{\mathbf{1}+(KC_e)^n} \quad (7)$$

where q_e is the amount of the CLF adsorbed at the interface at equilibrium, which is described by the fluorescence intensity of CLF. q_{max} is the maximum fluorescence intensity of the CLF at the SDS-laden LC/aqueous interface. C_e is the residual bulk concentration of CLF. K is the

adsorption constant for CLF. n is a measure of the heterogeneity of the surface. When n = 1, the adsorption is homogeneous. Our fitting result shows that n = 1.35, suggesting a heterogeneous adsorption of CLF molecules at the SDS-laden LC/aqueous interface by replacing the SDS at the interface. This result is consistent with the adsorption isotherm of bile salts at the protein stabilized oil/water interface in Euston's study, where the protein is displaced from the oil/water interface by bile salts [13]. The adsorption constant of CLF at the SDS-laden LC/aqueous interface is fitted to be 0.3 m^3 /mol. This is around 10 times smaller than the adsorption constant of bile salts at the protein stabilized oil/water interface [13], which is probably due to the much larger size of CLF compared to natural bile salts that makes CLF difficult to adsorb in the domains between SDS molecules at the SDS-laden LC/aqueous interface.

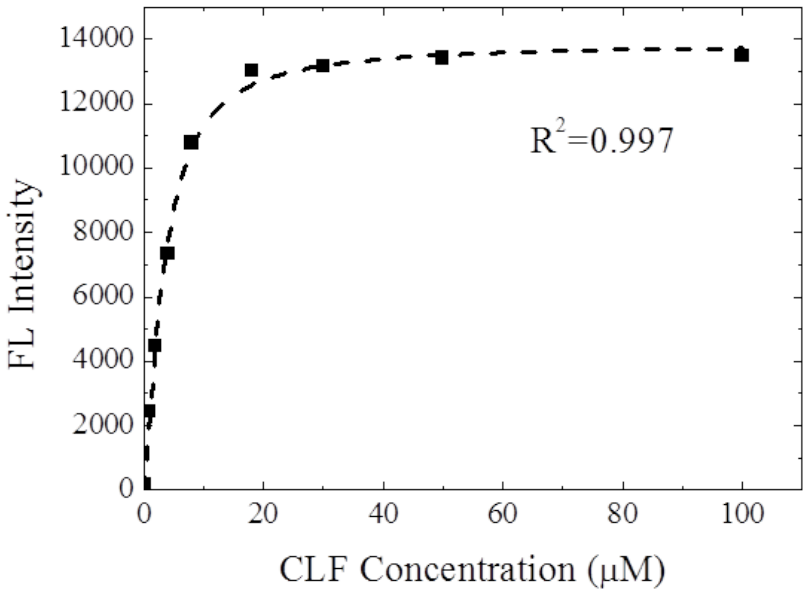

Figure 11: Fluorescence intensity of CLF at the SDS-laden LC/aqueous interface versus the bulk concentration of CLF.

2.3 Kinetics of the Adsorption of Bile Acids

Furthermore, we study the adsorption kinetics of CLF at the SDS-laden LC/aqueous interface by adding 0.15 μM CLF into the aqueous phase of the interface. Figure 12a shows the fluorescence intensity change at the interface as a function of time. We find that the fluorescence intensity increases rapidly at the beginning, then slows down to saturation. The adsorption kinetics can be fitted well by the pseudo-second order kinetics given by [66]

$$q(t) = \frac{k_2 q_e^2 t}{1+k_2 q_e t} \qquad (8)$$

where q(t) is the fluorescence intensity of the CLF at the interface at time t, q_e is the fluorescence intensity of CLF at equilibrium. k_2 is the rate constant for the second order kinetics, which is 0.006/hour from the fitting. The fitting with pseudo-second order kinetics shows R^2 = 0.993. It

has been found that the pseudo-first order kinetics is usually associated with chemisorption [67] and near equilibrium [66], while the pseudo-second order kinetics is associated with adsorption/desorption processes [67], which fits in our situation.

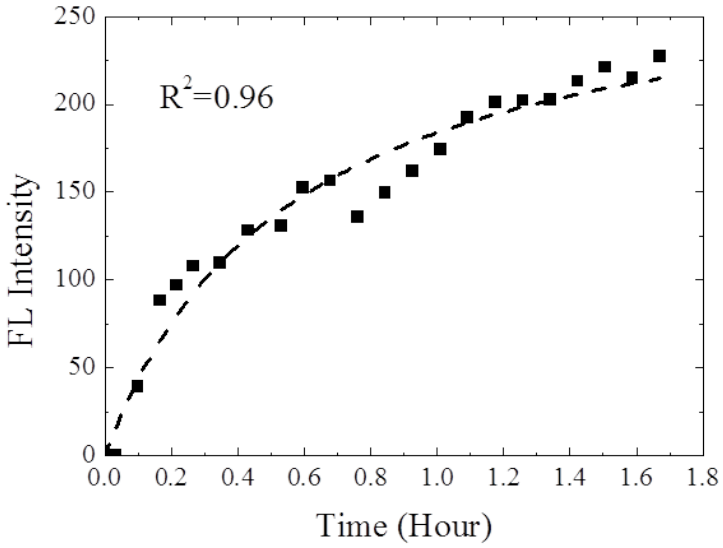

Figure 12: Fluorescence intensity of CLF at the SDS-laden LC/aqueous interface over time and its fitting using pseudo-second order kinetics. The LC here is 5CB. The concentration of CLF is 0.15 μM.

An interesting phenomenon is that the optical appearance of the SDS-laden LC/aqueous interface under polarizing microscope remains dark when the fluorescence intensity keeps increasing. The anchoring transition of the LC at the interface occurs after the fluorescence intensity levels off. This result suggests the displacement of the SDS at the interface requires the adsorption of CLF for a certain period of time. To further understand the displacement process, we study the time-dependent anchoring transition of LC at the SDS-laden LC/aqueous interface with the addition of CA [68].

The time-course polarizing microscopy images of the homeotropic-to-planar anchoring transition due to the competitive adsorption of CA were analyzed with NIH Image J, in which the transmission was calculated from the average brightness of the LC film in a square pore of the grid over time and then normalized to the maximum value. Thus, the polarizing microscopy observation is quantified in Figure 13 by plotting the normalized transmission as a function of time after the addition of CA, providing the information of the displacement kinetics of SDS from the LC/aqueous interface by the competitive adsorption of CA. The plots shown in Figure 13 reveal the lag-burst kinetics: a slow phase (termed as lag phase) followed by a rapid phase (termed as burst phase). The lag-phase should reflect the duration of the adsorption and penetration of CA at the SDS-laden LC/aqueous interface. The burst phase is a measure of the displacement of SDS from the LC/aqueous interface by CA. The slope of the plot of the burst phase represents the displacement rate of SDS from the LC/aqueous interface. It is clear in Figure 4 that the displacement rate increases with the increase of CA concentrations in the PBS aqueous phase. The lag time decreases from 10 hours to 1 hour when the concentration of CA increases from 4 μM to 40 μM. The increase of CA concentrations in the PBS aqueous phase should increase the availability of CA at the SDS-laden LC/aqueous interface, thus, shorting the lag time and enhancing the displacement rate. The displaced SDS from the LC/aqueous interface is solubilized by the CA remained in the aqueous phase through emulsification. The critical concentration of CA required to displacing the SDS from the LC/aqueous interface is ~ 1.5 μM [69]. There is no the homeotropic-to-planar anchoring transition of the LC at the interface observed for prolonged time periods (over 40 hours) if the concentration of CA is lower than ~ 1.5 μM.

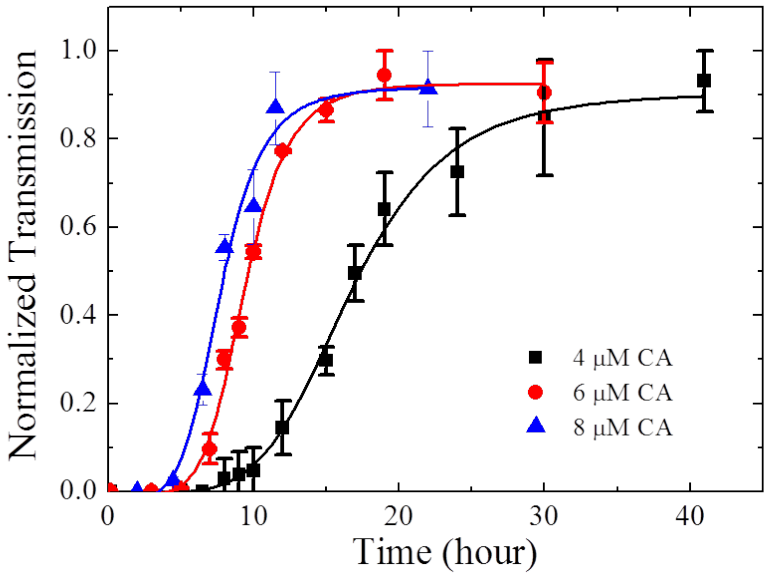

Figure 13: The normalized transmittance of the LC film confined in a pore of the grid as a function of time after the addition of 4 μM, 6 μM, 8 μM, and 40 μM CA at 25 °C. The LC here is a mixture of 5CB and 4-((4-propylphenyl)ethynyl)benzonitrile (5PCH) with 19 wt% 5PCH.

As we mentioned in Chapter 1, there are mainly two primary bile acids and two secondary bile acids in human. They are different in terms of the number and position of the hydroxyl group. To compare the adsorption of different bile acids, we plot the normalized transmission of the LC film confined in a square pore of the grid as a function of time after addition of 4 μM CA, 4 μM CDCA, 4 μM DCA, and 4 μM LCA, respectively (Figure 14) [68]. The order of the displacement rate (the slope of the plot of the burst phase) of the SDS from the LC/aqueous interface is LCA > CDCA > DCA > CA. The lag time is ~ 10 hours for 4 μM CA, ~ 60 min for 4 μM DCA, ~ 30 min for 4 μM CDCA and ~5 min for 4 μM LCA, respectively (Figure 14b). The order of the lag time is CA > DCA > CDCA > LCA. It is reasonable to expect

that the activity of these bile acids in the displacement of SDS from the LC/aqueous interface should correct to their hydrophobicity. Bile acids that are more hydrophobic should be less hydrated and therefore would more effective to penetrate into the SDS-laden LC/aqueous interface and more active to displace SDS from the interface. The order of hydrophobicity is LCA > DCA > CDCA > CA [70]. It is clear that there is an exchange in the order of the displacement rate between DCA and CDCA with respect to their hydrophobicity. It has been shown that the electrostatic interaction between bile acids and surfactants also plays an important role in the displacement of surfactants from the LC/aqueous interface [71]. The pKa is 6.1 for DCA and 6.3 for CDCA, respectively [72]. In the PBS aqueous phase at pH 7.4, the carboxylic acid group of both DCA and CDCA should be ionized. Thus, electrostatic interactions should not be a factor that causes the exchange in the order of the displacement rate between DCA and CDCA with respect to their hydrophobicity.

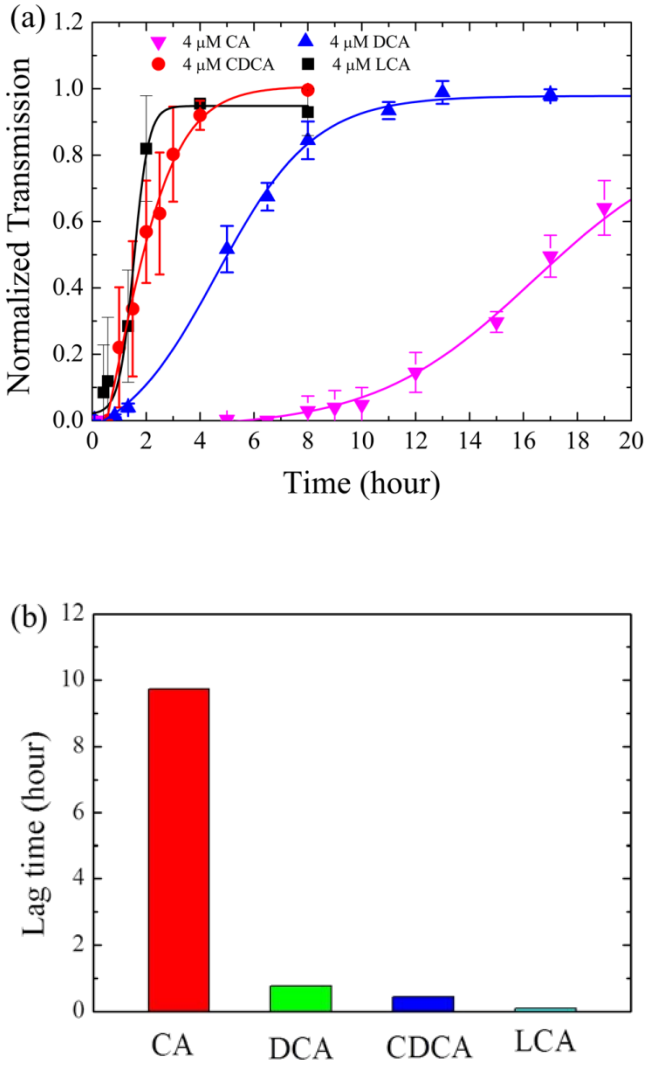

Figure 14: The normalized transmittance of the LC film confined in a pore of the grid as a function of time after the addition of 6 μM CA, 6 μM DCA, 6 μM CDCA and 6 μM LCA at 25 °C (a). Lag time of CA, DCA, CDCA and LCA (b).

As shown in Table 1, CDCA has two hydroxyl groups at C-3 and C-7 positions and DCA has two hydroxyl groups at C-3 and C-12 positions. We infer that the exchange between the C-12 and the C-7 position of the hydroxyl groups between DCA and CDCA may

overshadow their hydrophobicity in determining their activities in the displacement of SDS from the LC/aqueous interface. The interaction of SDS with CA, DCA and CDCA was studied by measuring the enthalpy change of the formation of mixed micelles [73]. The enthalpy change was found to be in the same order as the rate of the SDS displacement from the LC/aqueous interface, i.e., CDCA> DCA> CA. Thus, we conclude that CDCA with two hydroxyl groups at C-3 and C-7 positions are more favorable for interacting with SDS, compared to DCA with two hydroxyl groups at C-3 and C-12 positions. The energetic interaction makes CDCA more efficient in displacing the SDS from the LC/aqueous interface.

2.4 Special Optical Appearances Formed by the Adsorption of LCA

Besides the difference of the adsorption kinetics, the optical appearance of the LC films induced by bile acids are also different (Figure 15). For CA, DCA, and CDCA, the LC film show very dark brushes emanating from point defects, where the LC in the dark brushes aligns perpendicular or parallel to the polarizers. While for LCA, the brushes have much brighter optical appearance. This result shows that even though the LC at the interface in the brush region aligns perpendicular or parallel to the polarizers, there's a phase retardation in the region, suggesting that there is a twist deformation in the bulk LC phase. Since LCA is a chiral molecule with high hydrophobicity, we postulate that the twist deformation is due to the solvation of LCA in LC phase, which changes the nematic LC phase into cholesteric LC phase.

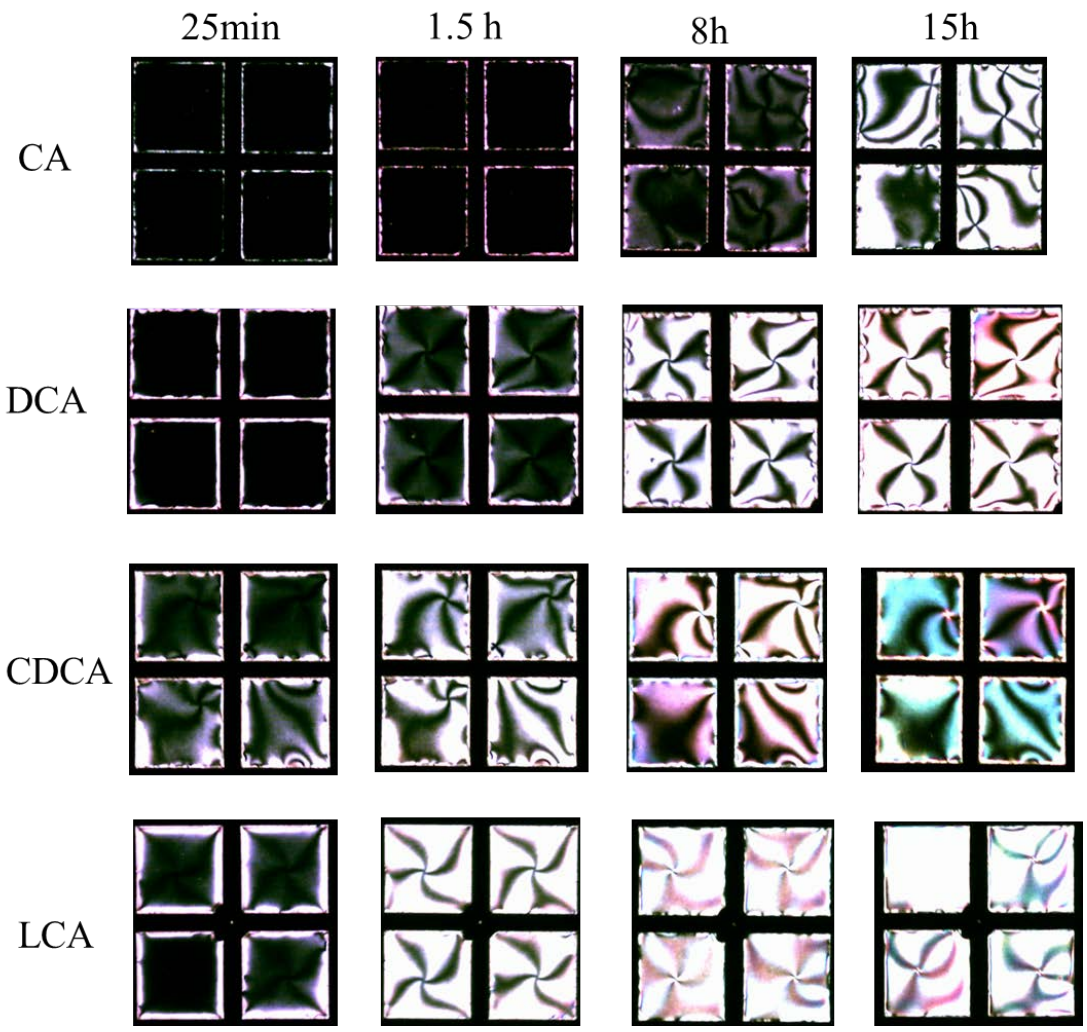

Figure 15: Polarizing optical microscopy images of the SDS-laden 5PCH/5CB mixture/aqueous interface after being exposed to 6 μM CA, DCA, CDCA, and LCA in PBS solution. Different rows show the exposure to different bile acids as notified on the left, and different columns show different exposure time as notified on the top.

The twist deformation of the LC film caused by the adsorption of LCA is more clearly shown in Figure 16, in which 5CB was used for the LC film to eliminate the any possible inhomogenerity of the 5PCH/5CB mixture. Here, the 5CB film was confined in the TEM grids and then exposed to 1.8 mM SDS solution without additional salts. Figure 16 a-c shows the same

change of optical appearances of LC film by the adsorption LCA as shown in Figure 15. Over time, we observe the formation of fingerprint textures, which are typical textures of cholesteric LCs in homeotropic or hybrid alignments. To further prove that this texture is due to the solvation of LCA in the LC film, we dissolve saturated LCA in 5CB (less than 1 wt% LCA), and make the LC film with the LCA/5CB mixture. Then we immerse the LCA/5CB film into 1.8 mM SDS solution. Indeed, we observe fingerprint textures.

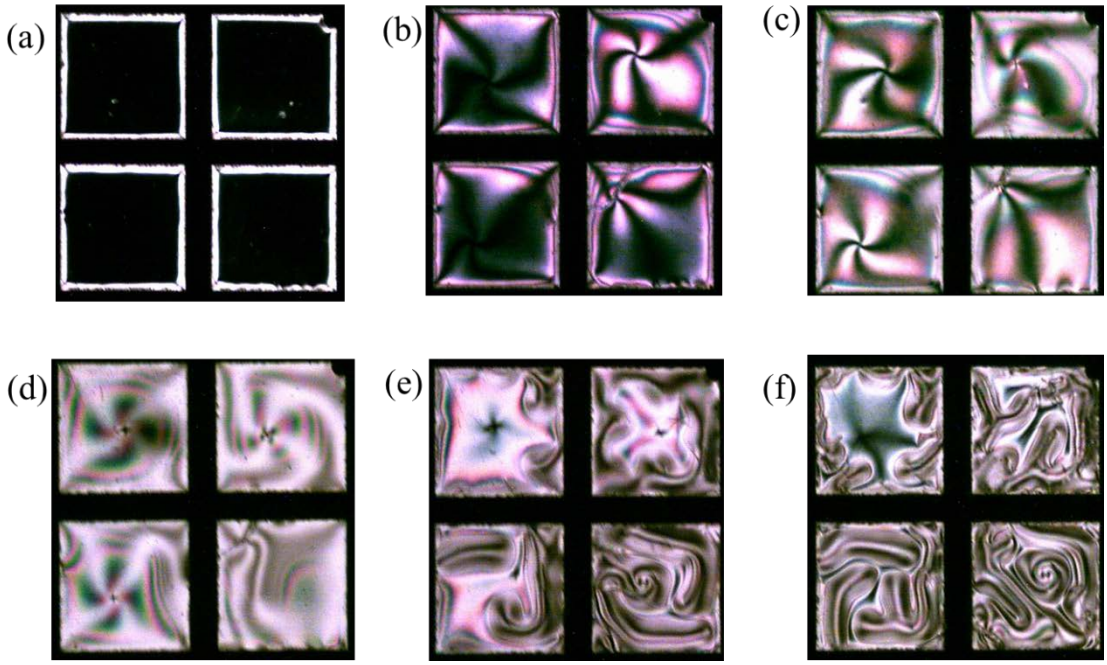

Figure 16: Polarizing optical microscopy images of the 5CB/aqueous interface in 1.8 mM SDS solution (a) without LCA; (b-f) with 28 µM LCA (pH ~ 8) for (b) 30min; (c) 1h; (d) 1.5h; (e) 2.5h; (f) 3h.

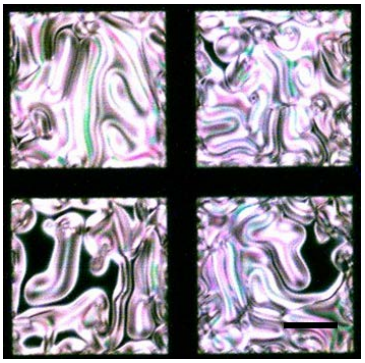

Figure 17: Polarizing optical microscopy images of the LC/aqueous interface in 1.8 mM SDS solution, where the LC is 5CB saturated by LCA.

The fingerprint textures of the 5CB film are not observed after the adsorption of CA, DCA, or CDCA at the SDS-laden nematic 5CB/aqueous interfaces. Our results suggest that LCA

has a high adsorption coefficient at the LC/aqueous interface due to its high hydrophobicity. This special pattern induced by LCA suggests that the 5CB film can be used to distinguish LCA from other bile acids.

2.5 Conclusion

In this chapter, the structure of LC-based biosensor and the detection mechanism for bile acids are discussed. The detection mechanism is due to the competitive adsorption of bile salt on SDS-laden LC/aqueous interface. This competitive adsorption can be fitted well with Langmuir-Freundlich adsorption isotherm. The fitting indicates that there is interaction between SDS and CA. The displacement of SDS from the LC-aqueous interface exhibits lag-burst kinetics. The lag time and the burst rate are found to depend on the number and position of the hydroxyl groups of bile acids. In the burst phase, the kinetics of adsorption of CA follows pseudo-second order kinetics. We also compare the optical patterns of the LC film formed by the adsorption of different bile acids. Unlike the adsorption of CA, DCA, and CDCA, the adsorption of LCA can lead to fingerprint textures. This special pattern of LCA is found to be the result of solvation of LCA in bulk LC phase.

CHAPTER 3 TUNABILITY OF DETECTION LIMIT

3.1 Influence of Detection Limit by Solution Conditions

In the last chapter, we investigated the detection mechanism. Here we want to study the impact of different part of the system on the detection limit. As shown in Figure 8d, our system consists of aqueous solution, surfactant, and liquid crystal. To study their impacts, we will first use the simplest LC 5CB and discuss the impact of the condition of aqueous solution, which includes pH and ionic strength.

As we mentioned in Chapter 2, the critical SDS concentration to induce a homeotropic alignment of LC is 1.8mM in deionized water. The minimum concentration (defined as the detection limit) of CA required to trigger the anchoring transition of the 5CB at the SDS-laden 5CB/aqueous interface is found to depend on the pH of the aqueous phase (Figure 18). When the pH value varies from 3.5 to 5.0, the detection limit for CA remains nearly unchanged (~ 12 μM). However, when the pH is above 5.0, the detection limit rapidly increases and reaches to ~ 170 μM at pH 7.5. The pH dependent detection limit is likely associated with the ionization of CA. The pKa of CA is measured to be ~ 5.0 [74]. When the pH of the aqueous phase is above 5.0, the carboxylic acid group of CA is expected to be ionized. Thus, the repulsive force between the negatively charged CA and the negatively charged SDS reduces the adsorption of CA at the 5CB/aqueous interface, leading to the increased detection limit of the SDS-laden 5CB/aqueous interface for CA.

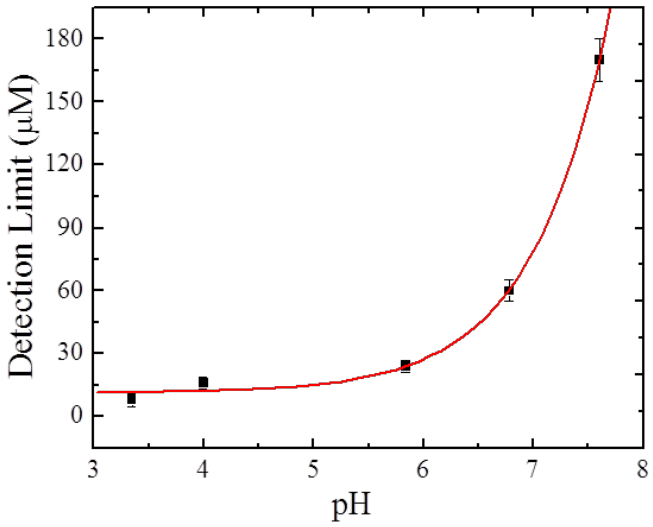

Figure 18: Detection limit of the SDS-laden 5CB/aqueous interface for CA as a function of pH values. The data points were obtained from three samples.

We further carried out the detection of CA in phosphate buffered saline (PBS) solution with an ionic strength of 172 mM and a pH of 7.4. In the PBS solution, only 50 μM SDS is needed to induce homeotropic alignment of 5CB. There are two effects contributing to the homeotropic alignment of 5CB at such low bulk concentration of SDS. One is due to the screening of electrostatic repulsion among the head groups of SDS by electrolytes, which leads to higher areal density of SDS at the 5CB/aqueous interface compared to that in pure 50 μM SDS solution without additional ions [50]. Another effect comes from the electric double layer formed by SDS at the interface and the electrolytes on the 5CB side of the interface. The internal electric field formed by the electric double layer can induce homeotropic alignment of 5CB [75]. In this PBS solution with 50 μM SDS, we find that the detection limit for CA has reduced to ~ 16 μM. The effect of the electrical double layer on the anchoring of the 5CB at the interface cannot

explain the decreased detection limit of the SDS-laden 5CB/aqueous interface in PBS solution. We infer that the decreased detection limit for CA in PBS solution may be a result of the charge screening of the anionic SDS at the 5CB/aqueous interface and the anionic CA in the aqueous phase at pH 7.4. Thus, the screening of the electrostatic interaction at high ionic strengths promotes the CA to penetrate into the SDS layer and disrupt the packing of SDS at the 5CB/aqueous interface. Consequently, the decreased detection limit for CA in PBS solution is observed.

3.2 Influence of Detection Limit by Surfactants

A typical tadpole-shaped surfactant is consisted of a hydrophilic head group and a hydrophobic carbon chain. It has been found that surfactants with shorter chain length can lead to a lower detection limit [76], and the shortest chain of commercial available surfactants that can induce homeotropic alignment of LC has 12 carbons [59]. For applications with low detection limit, we use surfactants with a 12-carbon chain and different head groups.

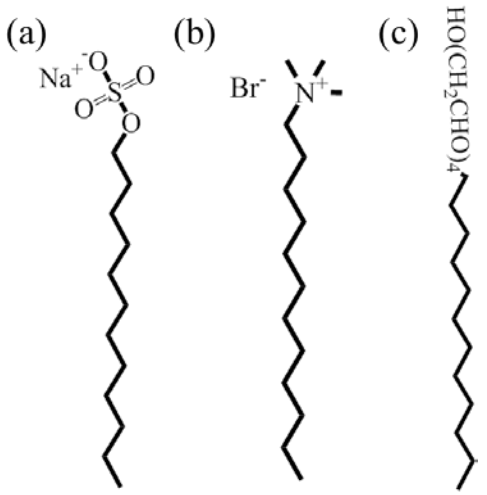

Figure 19: Chemical structures of SDS (a), DTAB (b), and $C_{12}E_4$ (c).

Figure 19 shows the chemical structures of SDS, dodecyl trimethyl ammonium bromide (DTAB) and tetra(ethylene glycol) monododecyl ether ($C_{12}E_4$), which have the same chain length but different head groups. DTAB has a positively charged head group, and $C_{12}E_4$ is neutral without charge. In deionized water, the concentrations required to induce homeotropic alignment of 5CB for SDS, DTAB and $C_{12}E_4$ are 1.8 mM, 7 mM and 30 μM, respectively. It has been shown that the limiting packing density at air/water interface follows: $C_{12}E_4$ (42 Å^2/molecule) < SDS (52 Å^2/molecule) < DTAB (63 Å^2/molecule) [59]. Therefore, only low concentration of $C_{12}E_4$ is needed to generate a densely packed $C_{12}E_4$ layer at the 5CB/aqueous interfaces, while a high concentration of DTAB solution is needed compared to SDS. The high critical concentration of DTAB is due to the large molecular head group and the electrostatic repulsion between the head group. From the calculation with software ChemDraw, the size of DTAB head group is ~ 22 Å^2, while the size of SDS head group is only ~ 15 Å^2. The low critical concentration of $C_{12}E_4$ is mainly due to the absence of electrostatic repulsion force. However, as

$C_{12}E_4$ has a very long chain in the head group, its head group can occupy a larger space than DTAB and SDS.

When CA is added to the aqueous phase side of the DTAB- and $C_{12}E_4$-laden 5CB/aqueous interfaces, we find no anchoring transition of the 5CB at the interfaces if the pH of the aqueous phase is above 5.0. This result suggests that the anionic CA is unable to disrupt the packing of the cationic DTAB and the nonionic $C_{12}E_4$ at the 5CB/aqueous interfaces. It is consistent with the above discussion that headgroups of DTAB and $C_{12}E_4$ pack more densely than SDS. For the DTAB-laden 5CB/aqueous interface, although there is electrostatic attraction between cationic DTAB and anionic CA, due to the densely packing of DTAB, CA may just adsorb on the cationic DTAB, rather than disrupt the DTAB at the 5CB/aqueous interface. When the pH of the aqueous phase is lower than 5.0, the anchoring transition of the 5CB at the DTAB- and $C_{12}E_4$-laden 5CB/aqueous interfaces is observed after being exposed to CA solution. For example, the detection limit of the DTAB- and $C_{12}E_4$ -laden 5CB/aqueous interfaces for CA at pH ~ 3.5 is found to be ~ 120 μM and ~ 200 μM, respectively (Figure 20a). This is consistent with the larger head group of $C_{12}E_4$ than DTAB, which makes it more difficult for CA to penetrate into the surfactant layer.

In PBS solution, the minimum concentration for DTAB to induce homeotropic alignment of 5CB is 1mM. Again, it is due to the screen of electrostatic repulsion among cationic headgroups of DTAB by electrolytes. In this case, ~ 100 μM CA can trigger the homeotropic-to-planar alignment of 5CB (Figure 20b). For $C_{12}E_4$, the addition of electrolytes does not reduce the minimum concentration to induce homeotropic alignment of 5CB, as $C_{12}E_4$ is non-charged. In this case, no transition of 5CB is observed for up to 200 μM CA.

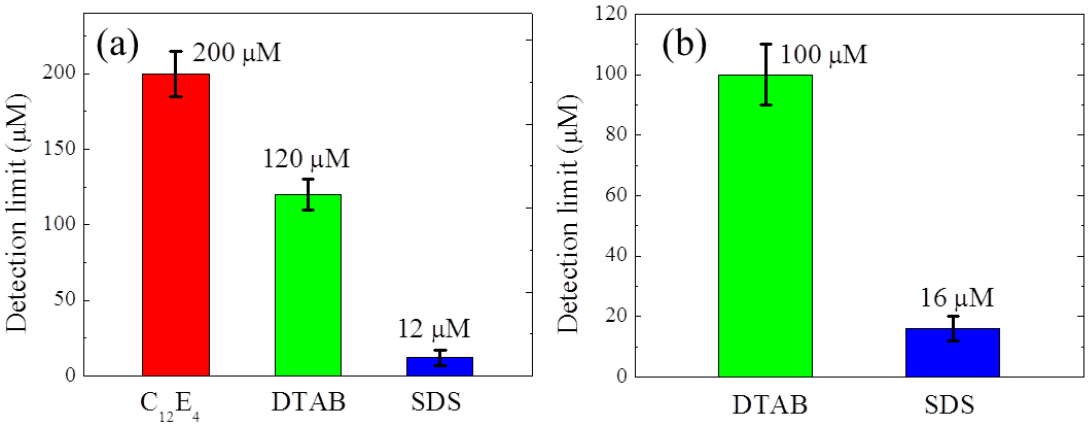

Figure 20: Detection limit of the surfactant-laden 5CB/aqueous interface for CA in aqueous solution with an ionic strength of 2 mM at pH 3.5 (a) and PBS with an ionic strength of 172 mM at pH 7.5 (b).

This shows the packing of head groups can strongly affect the adsorption of CA, as they sterically hinder CA adsorption. A similar effect was observed for bile acid adsorption at lipid/aqueous interface [11]. It was found that bile acids have less affinity for the non-ionic lipid/aqueous interface, and a better interfacial packing of the lipid head group makes it more difficult for bile acids to disrupt the lipid layer.

3.3 Influence of Detection Limit by Liquid Crystals

Liquid crystal is consisted of a rigid core, a headgroup and a tail (Figure 7). The rigid core is constructed from linearly linked rings, which can provide strong lateral interaction between molecules. Usually short terminal chains and weak polarity of head groups tend to generate nematic phase. When the terminal chain gets longer or the polarity of head groups gets

stronger, the dispersion force among long terminal chains and the electrostatic force among polar head groups tend to stabilize layer structure, which leads to formation of smectic phase.

The structures of LCs influence not only the interaction among these LC molecules which leads to different LC phases, but also the interaction between these LC molecules and the molecules on the LC surface. Therefore, in this chapter, we study the influence of LC materials on the detection of cholic acid. Based on the LC structure, the effect of chain length, core structure, and head group have been investigated.

3.3.1 Impact of Liquid Crystal Chain Lengths

In the last section, we conduct the detection using LC 5CB, which has a terminal chain with five carbons. Based on the detection mechanism of the competitive adsorption of CA at the SDS-laden LC/aqueous interface, a possible method of tuning the detection limit of the LC-based sensor platform for CA is to change the SDS/LC interaction at the interface by changing the nature of LCs. In this section, we study the effect of LC chain length.

The chemical structure of 4-n-alkyl-4′-cyanobiphenyl (nCB) is shown in Figure 21, with the temperature range is shown in Table 2.

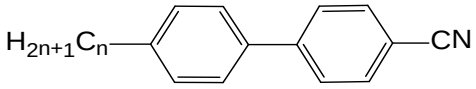

Figure 21: Chemical structure of nCB

Table 2 Phase transition temperatures of nCB. Cr denotes crystalline phase; S denotes smectic phase; N denotes nematic phase; I denotes isotropic phase. The phase transition data are obtained from a LC database Liq46 (LCI Publisher GmbH).

Liquid Crystals	Phase Transition Temperatures (°C)
5CB	Cr 23.5 N 35 I
6CB	Cr 14.5 N 29 I
7CB	Cr 30 N 42.8 I
8CB	Cr 21.5 S 33.5 N 40.5 I

Since the temperature of the nematic phase of nCB varies as a function of n (Table 2), we assembled nCB-based sensor platforms for the detection of CA at different temperatures to insure that nCB is in nematic phase. In our experiments, 50 μM SDS was added to into the aqueous phase side of the nCB/aqueous interface. After the homeotropic anchoring of the nCB at the interface was achieved by the adsorption of SDS at the interface, CA was added to the aqueous phase side of the SDS-laden nCB/aqueous interface. The detection limit for CA is found to linearly increase from 16 μM to 160 μM as the increase of n from 5 to 8 (Figure 22). We estimate that the detection limit for CA increases by ~ 51 μM per one additional carbon atom in the alkyl chain of nCB.

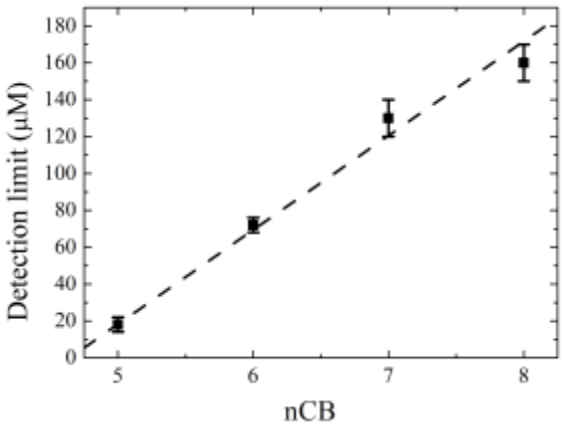

Figure 22: Detection limit of the SDS-laden nCB/aqueous interface for CA as a function of n in PBS solution. The detection was conducted at 25 °C for 5CB, 22 °C for 6CB, 32 °C for 7CB, and 36 °C for 8CB, respectively. The data points were obtained from three samples. The error bars represent the standard error.

Since the detection of nCB-based sensors for CA was carried out at different temperatures, we studied the influence of temperatures on the detection limit by performing the detection of 6CB- and 5CB-based sensors at different temperatures in the nematic phase of 6CB and 5CB, respectively. We find that there is no significant change in the detection limit observed when temperatures vary from 15 °C to 26 °C for 6CB and 24 °C to 33 °C for 5CB, respectively (Figure 23).

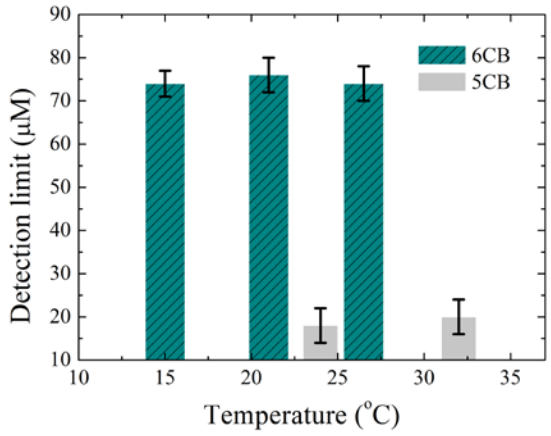

Figure 23: Detection limit of the SDS-laden 5CB/aqueous interface and the SDS-laden 6CB/aqueous interface for CA at different temperatures. The data points were obtained from three samples.

In Figure 22, the detection limit is 16 μM for 5CB and 130 μM for 7CB, respectively. The detection limit in this range can be further tuned by mixing 7CB with 5CB. The clearing temperature is 35 °C for 5CB and 42.8°C for 7CB, respectively. So we prepared 7CB/5CB mixtures with different mixed ratios at ~ 60 °C. The mixtures were then cooled down to ~ 24°C, at which the mixtures show nematic phase. Again, the adsorption of SDS at the 7CB/5CB mixture/aqueous interface induces homeotropic anchoring of the 7CB/5CB mixture at the interface. The removal of the SDS from the interface by the competitive adsorption of CA leads to a graduate change of the tilt angle of the mixture at the interface (Figure 24). The detection limit for CA is found to linearly increase from 16 μM to 130 μM when the 7CB/5CB mixed ratios increases.

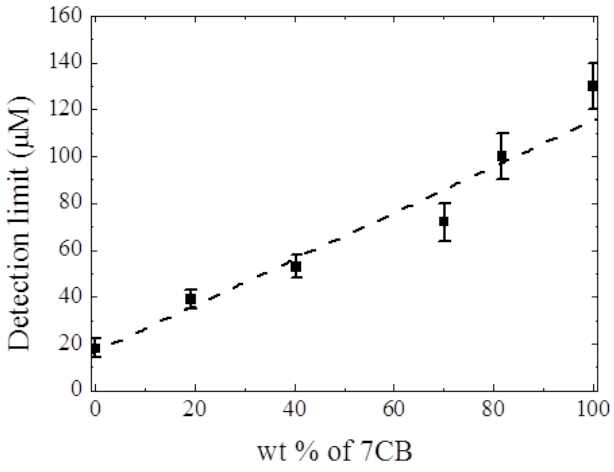

Figure 24: Detection limit of the SDS-laden 7CB/5CB mixture/aqueous interface for CA as a function of wt% of 7CB. The data points were obtained from three samples.

To compare the detection limit using nCB at room temperature, 20 wt% nCB are mixed with 5CB or 6CB, respectively. The results are shown in Figure 25. For nCB/5CB mixtures with $n \geq 5$, the detection limit almost linear increases with a slop of 10.23 μM CA per one additional carbon in the chain. For nCB/6CB mixture with $n \geq 5$, the detection limit also increases with the same slope of 10.23 μM CA per one additional carbon in the chain. This is consistent with the slope of detection limit for pure nCB, which is about five times higher than the mixtures with 20 wt% nCB. For $n \leq 4$, both nCB/5CB and nCB/6CB mixtures show a flat plateau. This may be because nCB do not have LC phase for $n \leq 4$. Therefore the interaction between LC and SDS is dominated by the host of 5CB or 6CB. The detection limits of nCB/6CB mixtures are ~ 40 μM higher than those of 5CB + nCB mixtures, which is consistent with the pure nCB experiment (Figure 22). As the detection limit of pure 6CB is ~ 50 μM higher than 5CB, thus the mixture of 80% 6CB + nCB is around 40μM higher than 80% 5CB + nCB.

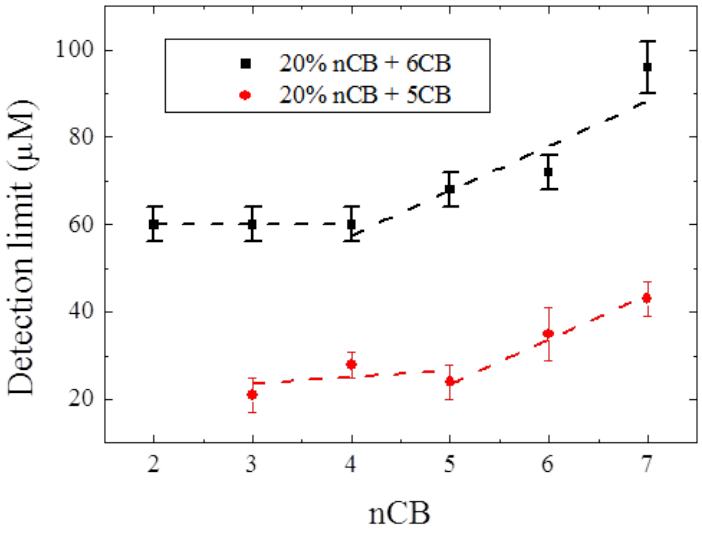

Figure 25: The detection limit of CA using LC mixtures at room temperature.

From the above linear relationship between detection limit of CA and weight percentage of nCB in nCB/5CB or nCB/6CB mixtures, we expect to be able to linearly tune the detection limit by changing the mixing ratio.

The orientation of LCs is known to be determined by the balance between the elastic energy and the surface anchoring energy. Thus, the changes in the elastic constant of nCB and/or the interaction of SDS with nCB at the interface are potentially factors that affect the detection limit for CA. Besides, birefringence of LCs may also affect the detection limit, as they can cause a greater phase retardation of light at the same tilted angle, which leads to greater light leakage at cross polarizers.

To find out the effects of elastic constants and birefringence, we measured the elastic constants and the birefringence of nCB/5CB mixture. First, we filled LCs into a homogeneous cell with 8μm cell gap at 80 °C through capillary force. Then a He-Ne laser (wavelength 633nm)

is normally incident through the polarizer, onto the cell, passing through the analyzer, and finally gets to the detector. A voltage of 0 to 5 V is applied vertically to the cell, and a voltage-dependent transmittance curve is obtained. The splay elastic constant is obtained from the Freederisksz transition threshold voltage V_{th} of LCs, where the LC director begins to deform,

$$K_{11} = \varepsilon_0 \Delta\varepsilon \left(\frac{V_{th}}{\pi} \right)^2 \quad (9)$$

where ε_0 is the vacuum permittivity, which is 8.854×10^{-12} F/m. $\Delta\varepsilon$ is the dielectric anisotropy. $\Delta\varepsilon$ of the LC mixture is obtained from the linear addition of $\Delta\varepsilon$ of each component, which is given by a LC database Liq46 (LCI Publisher GmbH). For 4-n-alkyl-4′-cyanobiphenyl (nCB) series, $\Delta\varepsilon$ (2CB) = 18.9, $\Delta\varepsilon$ (3CB) = 18.1, $\Delta\varepsilon$ (4CB) = 17, $\Delta\varepsilon$ (5CB) = 16.7, $\Delta\varepsilon$ (6CB) = 16.2, $\Delta\varepsilon$ (7CB) = 15.8.

Figure 26 shows that the elastic constants of nCB/5CB mixtures (n=5-8) alternately change with the increase of n, which is consistent with the trend of the elastic constant of pure nCB [77]. This odd-even effect of the elastic constant cannot explain the linear increase of the detection limit as the increase of n.

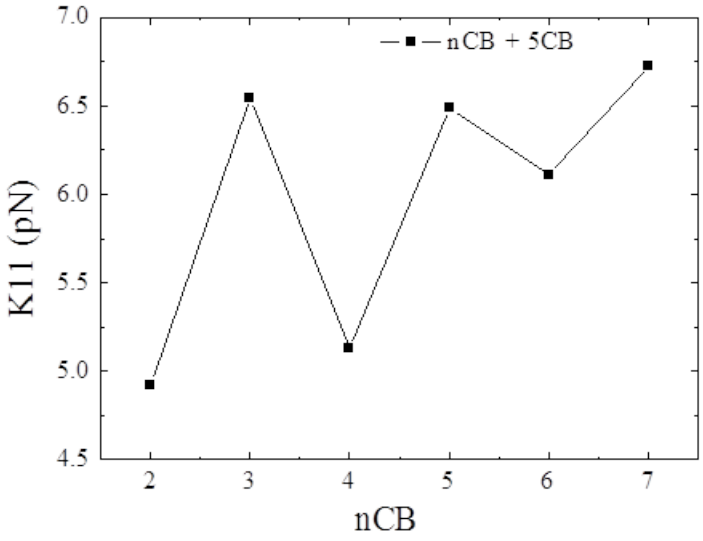

Figure 26: Splay elastic constant of 20 wt% nCB + 80 wt% 5CB mixtures.

The birefringence of nCB/5CB mixtures can be calculated from the phase retardation of the LC cell, which in turn was calculated from the voltage-dependent transmittance curve.

$$\Delta n = \frac{\theta\lambda}{2\pi d} \qquad (10)$$

$$\theta = 2\sin^{-1}(\sqrt{T}) \qquad (11)$$

where θ is the phase retardation of He-Ne laser beam passing through the LC cell, λ is the wavelength of the He-Ne laser (633nm), d is the cell gap (~8μm), and T is the transmittance. The birefringence of nCB/5CB mixtures is shown in Figure 27. It also shows an odd-even effect with the change of chain lengths, which is different from the trend of the detection limit for bile acids.

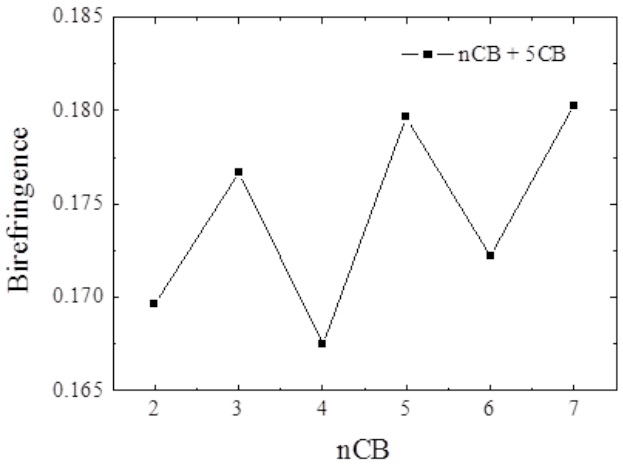

Figure 27: Birefringence of 20 wt% nCB + 80 wt% 5CB mixtures.

In the past, orientational wetting studies of nCB (n=5-9) on a surfactant-coated glass substrate showed that the partial-to-complete wetting transition of nCB occurred with the increase of n, indicating that the interaction of nCB with the surfactant increased with the increase of n [78, 79]. Thus, we conclude that the increased interaction between the SDS and the nCB at the interface makes the SDS more difficult to be removed by CA, leading to the increase of the detection limit for CA as the increase of n.

Because of the difference in the interaction of SDS with nCB, the interaction time and the optical patterns of the nCB film during the displacement of SDS are also different. Figure 28 shows the response of the 5CB film to 24μM CA in PBS solution. Over time, CA gradually replaces SDS and adsorbs at the 5CB/aqueous interface, which causes the 5CB molecules to be gradually tilted. Thus, the 5CB films turns bright over time. It takes about one hour for enough CA adsorbing onto the interface to trigger the transition of the 5CB film.

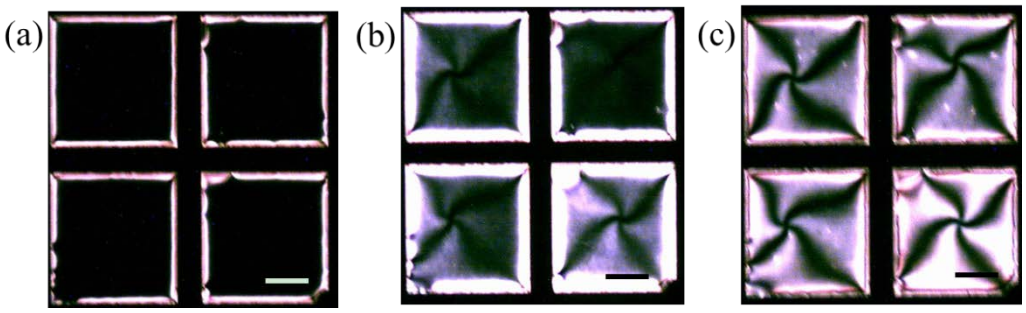

Figure 28: Polarizing optical microscopy images of the SDS-laden 5CB/aqueous interface after being exposed to 24 μM CA in PBS solution for 1 min (a), 1 hour (b), and 14 hours (c). Scale bar: 97 μm.

This response time depends on the concentration of CA. As CA concentration increases, the chance of CA to replace the SDS from the LC/aqueous interface also increases. Figure 29 shows that the SDS-laden 5CB film turns to fully bright within 3 min after being exposed to 80 μM CA in PBS solution.

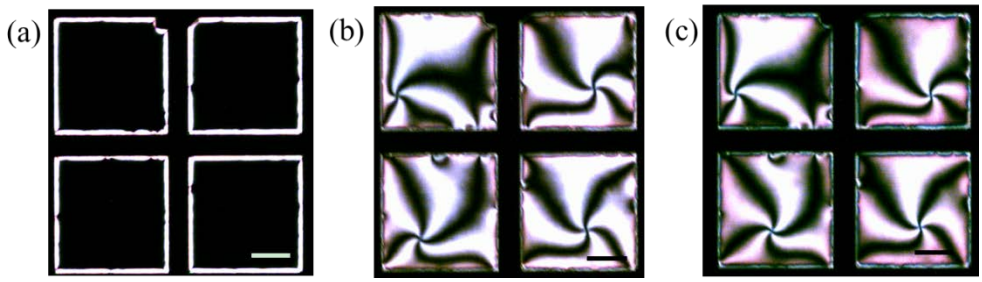

Figure 29: Polarizing optical microscopy images of the SDS-laden 5CB/aqueous interfaces after being exposed to 80 μM CA in PBS solution for 0 min (a), 3 min (b), and 20 min (c). Scale bar: 97 μm.

Compared with the SDS-laden 5CB/aqueous interface, the SDS-laden 6CB/aqueous interface shows slower replacement processes by 80 μM CA(9 min, Figure 30e). The optical pattern of the SDS-laden 6CB/aqueous interface is also quite different from the 5CB/aqueous

interface. For the 6CB/aqueous interface, there are clear boundaries between the domains of CA and SDS. This high heterogeneity of the interface indicates strong molecular interactions. As there is a strong interaction between 6CB and SDS, the original adsorption of SDS at the 6CB/aqueous interface may not be homogeneous. Therefore, CA molecules adsorb onto the discrete domains between SDS molecules where the packing density of SDS is low. The initially adsorbed CA molecules may act as nucleation sites. When more CA molecules move to the nucleation sites, the SDS adsorbed on the boundary of domains is displaced. Therefore, the CA domains keep growing, and finally merge together.

At the 7CB/aqueous and 8CB/aqueous interfaces, the similar replacement processes are observed, which is consistent with our proposed mechanism.

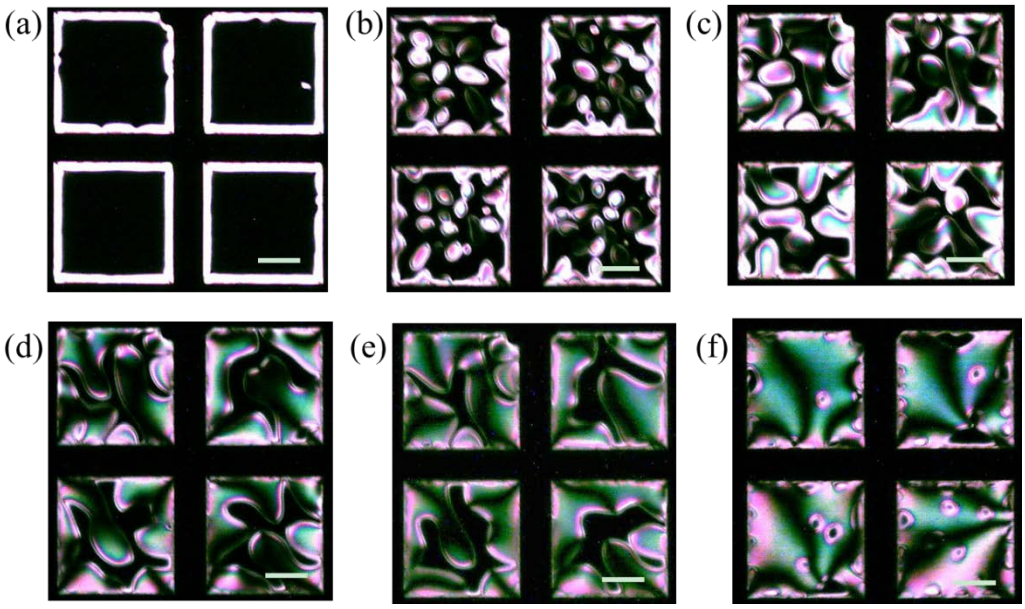

Figure 30: Polarizing optical microscopy images of the SDS-laden 6CB/aqueous interfaces after being exposed to 80 µM CA in PBS solution for 0 min (a), 5 min (b), 6 min (c), 7.5 min (d), 9 min (e), and 5 hours and 20 min. Scale bar: 97 µm.

3.3.2 Impact of Liquid Crystal Core Structures

To study the effect of core structure of LCs, we change the one or both phenyl rings of 5CB into cyclohexane rings, which gives 4-((4-propylphenyl)ethynyl)benzonitrile (5PCH, Figure 31a) and 4-(4-pentylcyclohexyl) cyclohexylcarbonitrile (5CCH, Figure 31b), respectively. Their nematic temperature range is shown in Table 3.

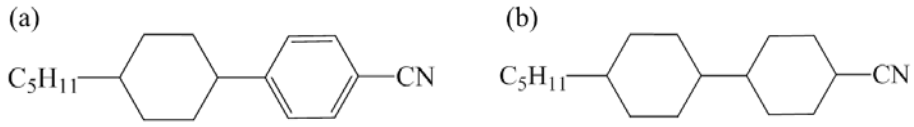

Figure 31: Chemical structures of 5PCH (a) and 5CCH (b).

Table 3 Phase transition temperatures of 5PCH and 5CCH. Cr denotes crystalline phase; S denotes smectic phase; N denotes nematic phase; I denotes isotropic phase. The phase transition data are obtained from a LC database Liq46 (LCI Publisher GmbH).

LCs	Phase Transition Temperatures (°C)
5PCH	Cr 31 N 55 I
5CCH	Cr 60 N 85 I

As compared to 5CB, 5PCH has a flexible and bulky core containing one phenyl ring and one cyclohexane ring. We find that the adsorption of SDS at the 5PCH/aqueous interface is unable to induce a homeotropic anchoring of the 5PCH at the interface. As can be seen in Figure 32a, a tilted anchoring of the 5PCH at the SDS-laden interface is achieved. The anchoring behavior of 5CB and 5PCH on lecithin monolayers formed by Langmuir-Blodgett technique was reported in the literature [80]. On densely packed lecithin monolayers, 5CB showed homeotropic anchoring, while 5PCH showed tilted anchoring, which agree with our results. It is likely that

flexible and bulky 5PCH requires higher anchoring energy to achieve homeotropic alignment than rigid 5CB. It has been shown that 5PCH and 5CB can form nematic mixtures over a wide range of mixed ratios [81]. We prepared 5PCH/5CB mixtures with different mixed ratios at ~ 70 °C. The mixtures were then cooled down to ~ 24°C, at which the mixtures show nematic phase. We find that the adsorption of SDS at the 5PCH/5CB mixture-aqueous interface can induce a homeotropic anchoring of the 5PCH/5CB mixtures with the mixed ratio up to 19 wt% of 5PCH (Figure 32b). Beyond this mixed ratio, SDS is unable to induce a homeotropic anchoring of the 5PCH/5CB mixtures at the interface.

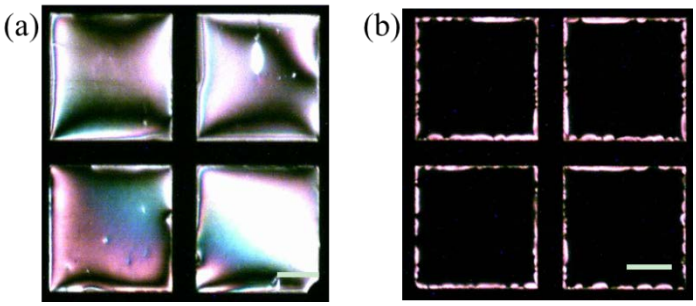

Figure 32: Polarizing optical microscopy images of the SDS-laden 5PCH/aqueous interface (a) and the SDS-laden 5PCH-5CB mixture/aqueous interface (b). The wt% of 5PCH in the mixture is 17 wt%. Scale bar: 97 µm.

Therefore, the CA detection by 5PCH/5CB mixture-based sensors was performed by using the 5PCH/5CB mixtures with the mixed ratios from 0 wt% to 19 wt% of 5PCH. The detection limit of 5PCH/5CB mixture-based sensors for CA is found to linearly decrease from 16 µM to 1.5 µM when the mixed ratio increases from 0 wt% to 19 wt% of 5PCH (Figure 33). It has been shown that the strong coupling of 5CB molecules is due to the large π-π interaction of their rigid cores (biphenyl rings) [82]. For 5PCH molecules, due to the presence of a bulky cyclohexane

ring in their core structures, they are weakly coupled. Thus, we expect a looser molecular packing in 5PCH/5CB mixtures, which makes the SDS more easily to be removed from the interface by CA, leading to the decrease of the detection limit.

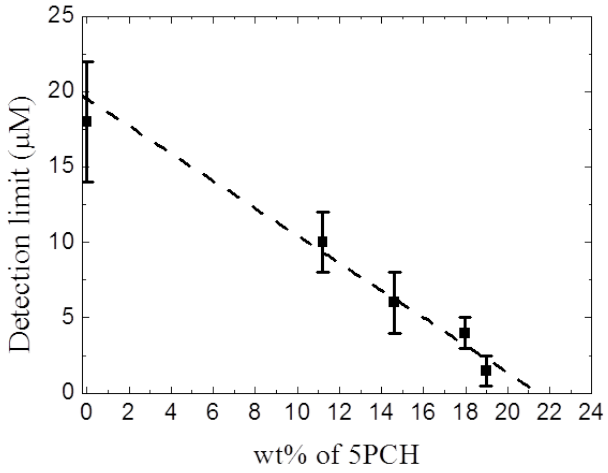

Figure 33: Detection limit of the SDS-laden 5PCH-5CB mixture/aqueous interface for CA as a function of wt% of 5PCH. The data points were obtained from three samples.

One would expect that if we change the other phenyl ring of 5CB into cyclohexane ring, the detection limit would be even lower. Therefore, we conducted the experiment using 5CCH. 5CCH contains two bulky cyclohexane rings in its core. The 5CCH/5CB mixture with different mixed ratios was prepared at ~ 90 °C and then cooled down to ~ 24°C. The adsorption of SDS at the 5CCH/5CB mixture-aqueous interface induced a homeotropic anchoring of the 5CCH/5CB mixture with the mixed ratio up to 16 wt% of 5CCH. As can be seen in Figure 34, the detection limit of 5CCH/5CB mixture-based sensors for CA linearly decreases from 16 μM to 6 μM with the increase of the mixed ratio from 0 wt% to 16wt% of 5PCH. The behavior of 5CCH/5CB mixtures in the detection of CA is similar to that of 5PCH/5CB mixtures, suggesting that an

additional cyclohexane ring in the core of 5CCH does not significantly affect the molecular packing in the mixtures.

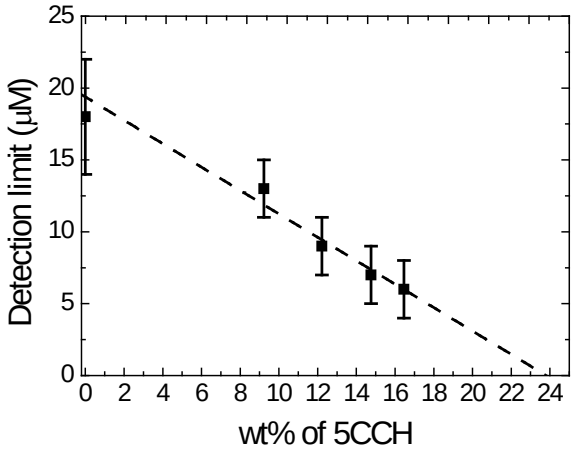

Figure 34: Detection limit of the SDS-laden 5CCH-5CB mixture/aqueous interface for CA as a function of wt% of 5CCH. The data points were obtained from three samples.

The clearing temperature (N-I transition) is 55°C for 5PCH and 85°C for 5CCH (Table 3), which is higher than that of 5CB (35°C). The clearing temperature of 5PCH/5CB and 5CCH/5CB mixtures linearly increases with wt% of 5PCH and 5CCH, respectively [81]. Thus, the LC-based sensors based on 5PCH/5CB and 5CCH/5CB mixtures can be operated in a much wider temperature range, compared to the 5CB-based sensors.

3.3.3 Impact of Liquid Crystal Headgroups

LCs with different head groups are also studied for the detection of CA. As most of them do not have nematic phase at room temperature, they are mixed with 5CB to form nematic phase at room temperature. The mixed ratio and detection limit in comparison with 5CB are shown in Table 4. The mixing ratios are chosen with reference to the eutectic mixing ratio, which is calculated by [81],

$$\frac{\Delta H_1}{\frac{\Delta H_1}{T_1} - R\ln X_1} = \frac{\Delta H_2}{\frac{\Delta H_2}{T_2} - R\ln X_2} \quad (12)$$

$$X_1 + X_2 = 1 \quad (13)$$

where ΔH is the heat enthalpy, "T" is the melting point, "R" is the gas constant (1.987 cal/mol/K), and X is mole fraction. The subscript denotes the component 1 or 2.

As the head groups change from –CN, to –NCS, and to C_3H_7, the detection limits increase. It is shown that –CN has a larger dipole moment (4.05 Debye) than –NCS (3.4 Debye), and C_3H_7 has negligible dipole moment [83]. The large dipole moment tend to make LC molecules align antiparallely, while only LC molecules that align with tails towards the LC/aqueous interface can interact with the tails of SDS efficiently. Hence a large dipole moment may inhibit the orientation of LC molecules to rotate with tails towards the SDS monolayer, thereby reducing the tail-tail interaction between LC and SDS, which makes it easier for CA to replace SDS from the interface.

Table 4 Detection limit using LCs with different headgroups. The weight percentage in the bracket on the left denotes the percentage of this material in its mixture with 5CB.

Name	Structure	Detection limit (μM)
5CB		16
PP-5NCS (17.9 wt%)		40
PP-53 (16.72 wt%)		85

3.4 Conclusion

By studying the influence of pH, ionic strength in aqueous solution, head groups of surfactants, and LC structures, we showed that a wide range of tunable detection limits could be achieved. The 5CB-based sensor has a lowest detection limit (~16 μM) for CA. The detection limit of nCB-based sensors for CA linearly decreases from 160 μM to 16 μM when the alkyl chain length of nCB is reduced from n=8 to n=5. By using 5PCH/5CB mixtures, the detection limit for CA can be further reduced from 16 μM to 1.5 μM linearly when the mixed ratio increases from 0 wt% to 19 wt% of 5PCH.

CHAPTER 4 DETECTION OF BILE ACIDS IN URINE

4.1 Detection of Bile Acids in Synthetic Urine

In Chapter 3, we showed that the 5PCH/5CB mixture with 19% 5PCH gives the lowest detection limit for CA. Therefore, we use this mixture for the detection of bile acids in synthetic urine. The synthetic urine is purchased from Ricca Chemical Company (Arlington, TX). Table 5 shows the components in synthetic urine. The effect of salts was discussed in Chapter 3. Thus, the only possible interfering specie for the detection of bile acids in synthetic urine is urea (Figure 35a). Urea is very hydrophilic, and forms hydrogen bonding with water [84]. It has been found that urea would reduce the surface polarity of the micelles of ionic surfactants [85]. In our experiment, we find that 50 μM SDS in synthetic urine also induce the homeotropic alignment of the LC at the interface, although the ionic strength of synthetic urine is lower than that of PBS solution. The improvement of the adsorption of SDS at the LC/aqueous interface can be due to the decrease of the surface polarity of SDS at the interface in the present of urea. This improvement of the adsorption of SDS leads to the increase of detection limit of CA to 46 μM.

Table 5 Components in synthetic urine

Components	**Concentration**
$MgSO_4 \cdot 7H_2O$	3.65 – 4.87 mM
$CaCl_2$	< 9.01mM
NaCl	102 – 171mM
Urea	283 -350 mM

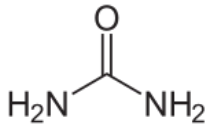

Figure 35: Chemical structure of urea.

The detection limit of the LC-based biosensors for different bile acids in synthetic urine is shown in Figure 36a. The detection limit here is determined by the transition of the optical appearance of LC biosensor in 2 hours. The order of the detection limit for CA, DCA, and CDCA is the same as in PBS solution. Furthermore, we detect taurolithocholic acid 3-sulfate disodium salt (Sulfated NaTLC, Figure 36b) in synthetic urine because sulfated bile salts occupy 60% of total bile salts in urine [26, 86]. Compared to CA and DCA, sulfated NaTLC replaces the hydroxyl group at C-3 position by sulfate group, which greatly reduces its hydrophobicity, but the lack of hydroxyl group at C-7 and C-12 position helps to increase its hydrophobicity. The balance between these two effects places the detection limit of sulfated NaTLC between CA and DCA.

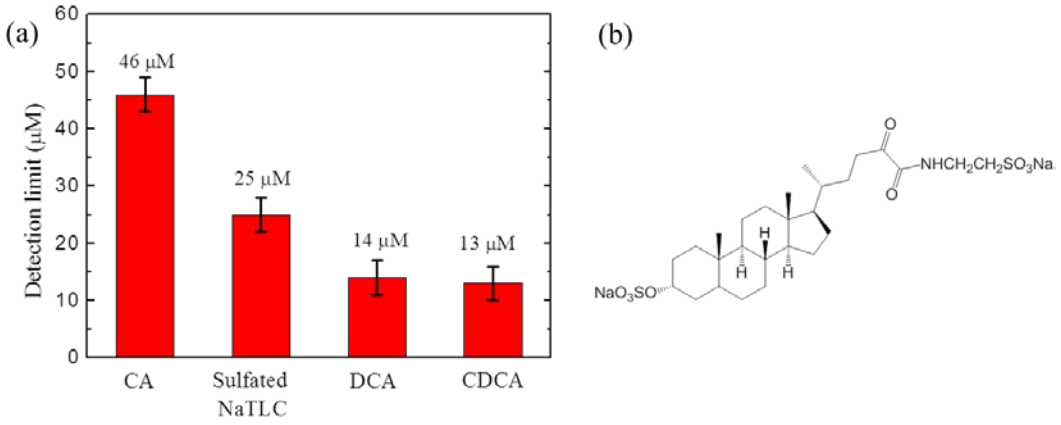

Figure 36: Detection limit of the mixed LC-based biosensors for different bile acids in synthetic urine (a) and chemical structure of sulfated NaTLC (b).

Since the detection limit for sulfated NaTLC (25 μM) is above the criteria for abnormal urinary bile acid concentration (10 μM), we need to reduce the detection limit. As we showed in Chapter 3, the detection limit can be tuned by different components in the detection system. Now we change the concentration of SDS to reduce the detection limit. Figure 37 shows the detection limit for NaTLC almost linearly decreases with decreasing SDS concentrations. By reducing the SDS concentration to 10 μM , the detection limit for sulfated NaTLC can be reduced to 1μM.

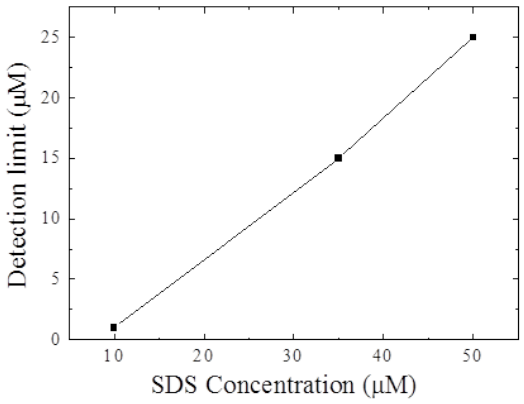

Figure 37: Detection limit for sulfated NaTLC as a function of SDS concentrations.

4.2 Detection of Bile Acids in Human Urine

Finally, we detect bile acids in human urine with the LC-based biosensors. Human urine was from the healthy author and then filtered with 0.22 μm pore size filters to remove some cells and large proteins. Compared with synthetic urine, human urine has more potential interfering species. Besides urea, another two major components in urine are creatinine and uric acid [87] (Figure 38a, b). To find out the effect of these two components, we carry the detection in the presence and absence of both components. We find that the LC based biosensors show no response to them even at concentrations higher than normal concentrations (Figure 39a, c). We further test the sensitivity of the LC biosensor for bile acids in synthetic urine with and without creatinine and uric acid. The detection limit for bile acids is found to be unaffected by the presence of creatinine and uric acid (Figure 39b, d).

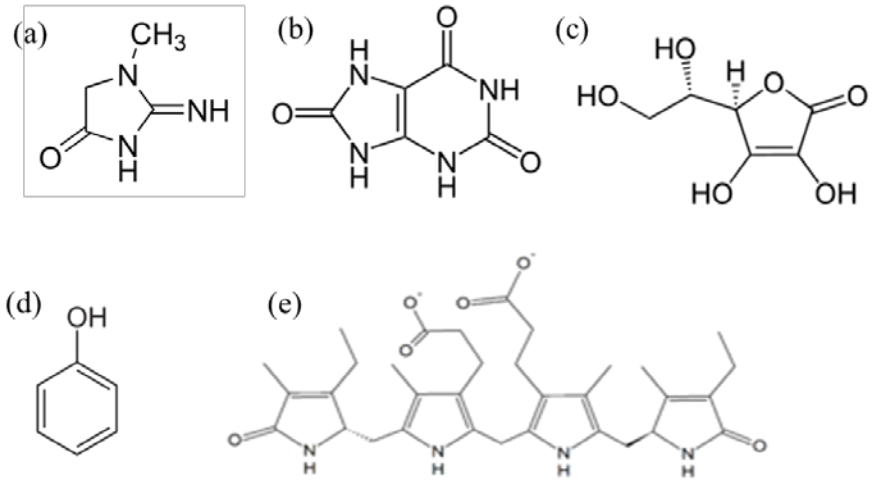

Figure 38: Chemical structures of possible interfering species in urine: creatinine (a), uric acid (b), ascorbic acid (c), phenol (d), and urobilinogen (e).

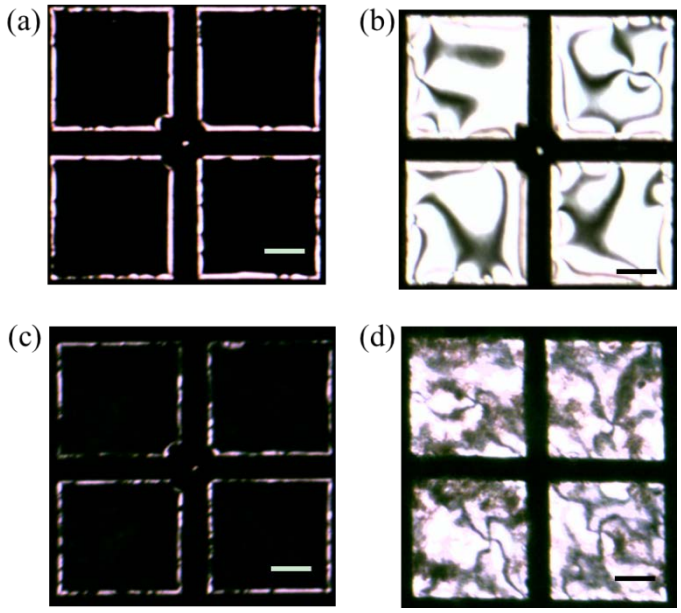

Figure 39: Polarizing microscopy images of the SDS-laden LC/aqueous interface before (a, c) and after (b, d) the exposure to 1 µM sulfated NaTLC for 30 min in synthetic urine with (c, d) and without (a, b) 10 µM creatinine and saturated uric acid. Normal concentration of creatinine is 9 µM. Scale bar: 97 µm.

The other possible interfering species are ascorbic acid (Figure 38c), phenol (Figure 38d), and urobilinogen (Figure 38e). The normal concentration of phenol is 100 ± 38.3 μM [88], and the concentration of urobilinogen in this urine sample was tested using a urine test strip and found to be 3.5 μM, which is within the normal range (< 17μM) [89]. To test the interference of these species, we conduct the tests in synthetic urine with urobilinogen, phenol, and ascorbic acid, respectively. We find that the LC-based biosensor is insensitive to 100 μM phenol and 240 μM ascorbic acid, respectively. However, the LC-based biosensor does response to 3.5 μM urobilinogen. This is probably due to the amphiphilic nature of urobilinogen, which also competitively adsorbs at the SDS-laden LC/aqueous interface. To eliminate the effect of urobilinogen, we increase the SDS concentration and find the densely packed of SDS can prevent the effect of urobilinogen. For example, when the SDS concentration is increased to 230 μM, the LC-based biosensor shows no response (dark) to the addition of 7 μM (in normal range) sulfated NaTLC in urine (Figure 40a), while it changes to bright appearance with 10 μM (in normal range) sulfated NaTLC in urine (Figure 40b). Our results show the potential of the LC-based biosensor for the detection of urinary bile acids.

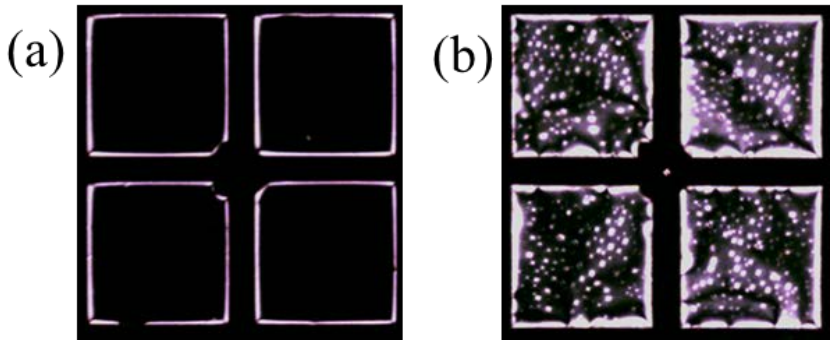

Figure 40: Polarizing optical microscopy images of LC biosensors in human urine after the addition of 7 μM sulfated NaTLC (a) and 10 μM sulfated NaTLC for 30 min (b).

4.3 Conclusion

In this chapter, we analyzed the effects of multiple possible interfering species for the detection of bile acids with the LC-based sensor in urine. We find that the major components urea, creatinine, and uric acid, as well as minor components ascorbic acid and phenol, would not trigger the orientational transition of the LC at the interface. But urobilinogen could trigger the orientational transition of the LC at the interface. Since the concentration of urobilinogen could be easily found out using a test strip, we could pretreat the LC-based biosensor to compensate the effect caused by urobilinogen. One simple method is to increase the SDS concentration. We found that by increasing the SDS concentration to 230 μM, the LC-based biosensor could response to the sulfated bile acid above normal concentration in 30 min, which demonstrates the potential for self-examination of liver dysfunction.

CHAPTER 5 FURTHER APPLICATION: DETECTION OF LIPOLYSIS

5.1 Introduction to the Impact of Bile Salts on Lipolysis Processes

As we have shown in Chapter 1, bile salts play a very important role in the digestion of lipid and lipid-soluble vitamins. However, the detail on how bile salts affect the lipolysis by pancreatic lipase in intestine is still controversial. The study of bile salts on the lipolysis by pancreatic lipase can be dated back as early as 1891 when Rachord found that bile or glycocholate can enhance the lipolysis of olive oil by pancreatic juice [90]. But this role of bile salts has been a long-standing argument ever since then. In 1923, Willstatter and Memmen showed the inhibition effect of bile salts on the lipolysis [91]. Recently, it is reported that bile salts enhance the lipase activity at low bile salt concentrations (≤ CMC of bile salt), but inhibit the lipase activity at high bile salt concentrations [92]. However, the lypolysis is a very complex process, and the role of bile salts not only depends on its own concentration, the type of bile salts [93, 94], but also pH [93], temperature [95], colipase [95], calcium ions [96], and so on. The influence is explained as the result of the formation of lipase-bile salt complexes [97], electrostatic interaction [98], surface tension [99], and the activation of lipase [92]. In this study, we find that the incubation time of the substrate in bile salt solution also affects the lipolysis, and bile salt at high concentration (> CMC) can accelerate the lipase activity due to the disruption of densely packed substrates and the displacement of lipolysis products.

There are several methods to monitor the hydrolysis of lipids, such as titration of the liberated fatty acid in a lipid emulsion [96, 100], fluorescence shift as a fluorescent compound binds to hydrolysis products [101], atomic force microscopy of the degradation of the phospholipid layers [102], chromatography analysis [103], quartz-crystal microbalance [104], and IR

reflection absorption spectroscopy [105]. Compared to the study of the hydrolysis in emulsions, the image of the hydrolysis of a phospholipid layer gives detailed information about the hydrolysis kinetic process. Most of these studies are conducted at the air/water interface. Here we use a LC-based biosensor to study the hydrolysis at the liquid crystal/aqueous interface.

5.2 Study of the Impact of Bile Salts on Lipolysis Processes Using LC-based Biosensors

It was recently discovered that porcine pancreatic lipase (PPL) can catalyze the hydrolysis of phospholipids. PPL can accommodate a phospholipid molecule in its active site and possesses phospholipase A_1 activity [106]. The hydrolysis of 1,2-dipalmitoyl-sn-glycero-3-phosphocholine (L-DPPC) by PPL is shown in Figure 41, where PPL catalyzes the fatty acid cleavage in the sn-1 position of L-DPPC.

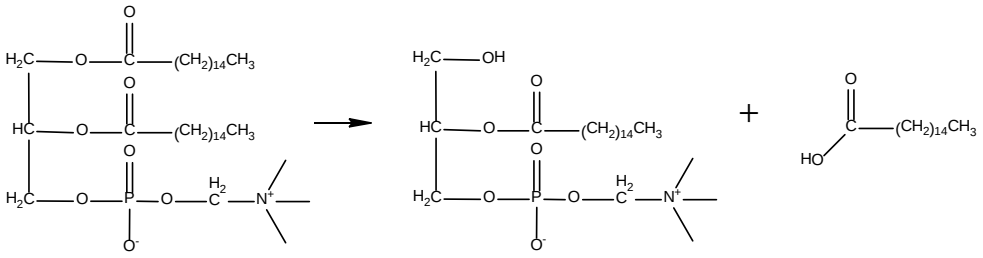

Figure 41: Hydrolysis of L-DPPC catalyzed by PPL.

To make the DPPC-laden LC/aqueous interface, we immerse the LC film confined in TEM grids supported by a polyimide-coated glass substrate into 0.1mM DPPC emulsion. The adsorption of DPPC at the LC/aqueous interface induces a homeotropic alignment of the LC at the interface, which gives a dark appearance under a polarizing optical microscope [31, 52, 107]. To remove the excess DPPC from the upper aqueous phase, we exchange the upper solution with water. The LC film remains dark, which indicates that the DPPC adsorbed at the

LC/aqueous interface remains stable [52]. Addition of 80 nM PPT into the aqueous phase does not lead to a change of the optical appearance of the DPPC-laden LC film, indicating that the hydrolysis does not happen. Since DPPC exists in a solid-like gel state at room temperature [108], it is difficult for PPL to interact with DPPC at the LC/aqueous interface. It is found that NaTDC is very effective to displace phospholipids from oil-water interface, compared to other bile salts [98]. Therefore, we chose NaTDC in our study. NaTDC is added to the aqueous side of the DPPC-laden LC/aqueous interface. After 3 hours, we remove the NaTDC remained in the upper aqueous phase by exchanging the aqueous solution with water. Afterwards, we add PPT into the aqueous side of the DPPC-laden LC/aqueous interface. The CMC of NaTDC is 2 mM [109]. We find that there is no lipolysis observed within 12 hours after the addition of 1 mM NaTDC. However, when the concentration of NaTDC increases to 5mM, the lipolysis of DPPC is observed, which is indicated by the change of optical appearance of the liquid crystal film (Figure 42). As PPL is introduced into the upper aqueous phase, it adsorbs onto the DPPC layer at the LC/aqueous interface to create some nucleation sites where the hydrolysis occurs (Figure 42b), which triggers the perpendicular-to-tilt anchoring transition of the LC at the interface, as indicated by the formation of bright domains. These domains gradually move to the edge of the grid because of the elasticity of LCs (Figure 42c). It has been found that the elastic energy of LCs was large enough to induce phase separation of a lipid layer at the liquid crystal/aqueous interface [110]. In our experiment, the LCs align in a planar direction at the edge of the grid. To reduce the elastic energy, LCs drive the planar domains from the center to the edge. As the hydrolysis process goes on, the bright domains become larger and eventually covers the whole grid (Figure 42f).

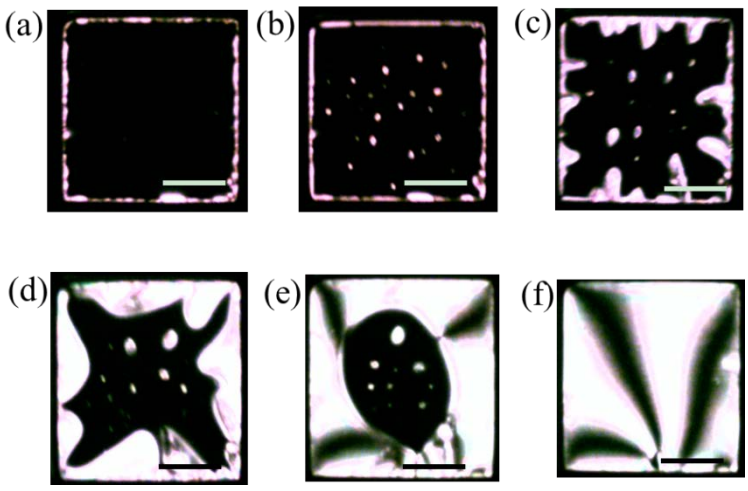

Figure 42: Polarizing optical microscopy images of the DPPC-laden LC/aqueous interface before (a) and after being exposed to 80 nM PPL at 22°C for 5 hours (b), 8.5 hours (c), 13 hours (d), 16 hours (e), and 25 hours (f). Scale bar: 97 μm.

There are two hypotheses here. First, we hypothesize that the role of NaTDC is to displace some DPPC molecules from the LC/aqueous interface, which lowers the packing density of the DPPC at the interface. Second, we hypothesize that the exchange of the upper aqueous solution with water removes most of the NaTDC at the interface as well as the NaTDC in the upper aqueous solution. The first hypothesis is based on the zeta potential [98] and surface tension measurements [111], which show that NaTDC can completely displace all phospholipids at the oil/water interface. The second hypothesis is based on the studies showing that surfactant with high solubility can easily desorb from the LC/aqueous interface by lowering its bulk concentration [50, 52] and NaTDC is highly soluble (10mg/mL in water). To verify these hypotheses, we compare the above lipolysis process to another case where the DPPC-laden LC/aqueous interface is formed by the incubation in 2μM DPPC solution until the LC film shows dark appearance (Figure 43). The polarizing microscopy observation is

quantified by plotting the normalized bright area as a function of time after the addition of PPL. The first case with high DPPC concentrations (0.1mM bulk solution) followed by 3 hour incubation in NaTDC solution shows the same lipolysis process as the second case where the loosely packed DPPC is formed at the interface by the incubation of the LC film in low DPPC bulk solution (2 μM) without the incubation in NaTDC solution. This indicates that these two cases are in the same condition, which supports our two hypotheses. In both cases, the plot reveals the lag-burst kinetics: a slow phase (termed as lag phase) followed by a rapid phase (termed as burst phase). The lag-phase should reflect the duration of the adsorption and penetration of PPL at the DPPC-laden LC/aqueous interface, corresponding to the dark image in Figure 42a. The burst phase is a measure of the hydrolysis of DPPC. The slope of the plot of the burst phase represents the hydrolysis rate.

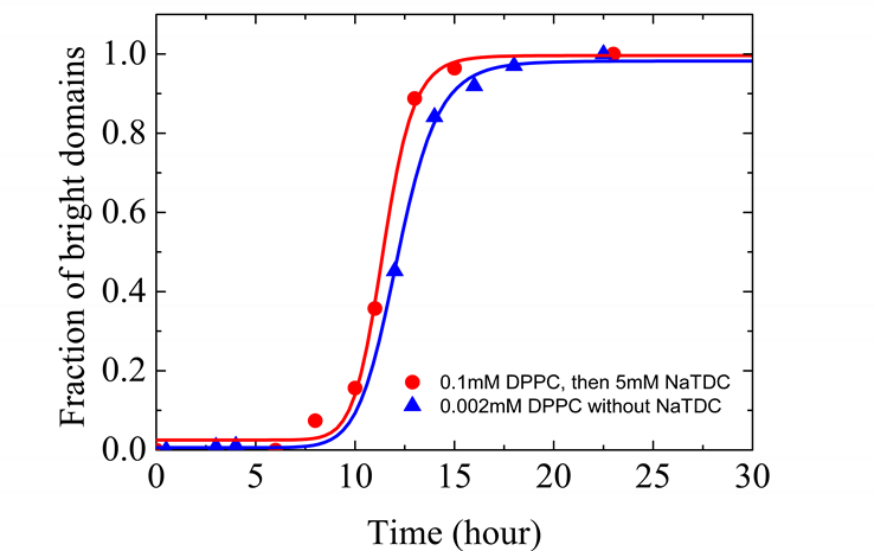

Figure 43: Fraction of bright domains at the LC/aqueous interface under polarizing optical microscope for the hydrolysis of lipid by 50 nM lipase and 50nM colipase. For the red curve, the DPPC-laden interface is formed by the incubation of a LC film in 0.1 mM bulk DPPC emulsion, exchanged with water, and then incubated in 5mM NaTDC solution for 3 hours and exchanged with water before the addition of lipase (red circle). For the blue curve, the DPPC-laden interface is formed by the incubation of a LC film in 0.002 mM bulk DPPC emulsion, and then exchanged with water. No NaTDC is added.

To study the role of NaTDC in the lipolysis of DPPC, we compare three samples (Figure 44). All these three samples have the DPPC-laden LC/aqueous interface made by the incubation in 0.1 mM DPPC for one hour. The DPPC solution was then exchanged with water. The first sample (black square in Figure 44) was further incubated in 5mM NaTDC solution for 3 hours. Then the NaTDC solution was exchanged with water before the addition of 80 nM PPL. The second sample (red circle in Figure 44) was incubated in 5mM NaTDC solution

for 3 hours, followed by the addition of PPL without exchanging the NaTDC solution with water. The third sample (blue triangle in Figure 44) was made by the addition of both 5mM NaTDC and PPL at the same time. The lag phase of the first sample without NaTDC during the lipolysis lasts 2 hours, while for the second and third samples with NaTDC, the lag phase lasts 4 hours (red circle and blue triangle in Figure 44). This shows that the excess NaTDC in the solution prolongs the lag time. There were many studies showing that bile salts at the interface can inhibit the adsorption of lipase onto the substrate due to the competitive adsorption [94, 99, 112]. If this is the case, the lag time for the sample which NaTDC is added at the same time with PPL should be shorter than the sample which is incubated in NaTDC solution for 3 hours before the addition of PPL, as the former sample has less NaTDC at the interface due to shorter incubation time. Therefore, we infer that the lag time is a result of the presence of NaTDC in the aqueous phase rather than at the interface. The slope of the plot represents the hydrolysis rate of the burst phase. Figure 44 shows that the hydrolysis rate follows: first sample < third sample < second sample. As NaTDC in the first sample was removed, we expect the first sample has the least NaTDC at the interface. The third sample has much shorter incubation time in NaTDC solution than the second sample, so we expect the third sample has less NaTDC at the interface than the second sample. The trend of the hydrolysis tells that more NaTDC at the interface can promote the lipolysis DPPC. There could be two reasons. One is that NaTDC at the interface helps remove lipolysis products from the interface [92, 113]; another is that NaTDC induces the opening of lipase lid, which promote the hydrolysis [92, 114].

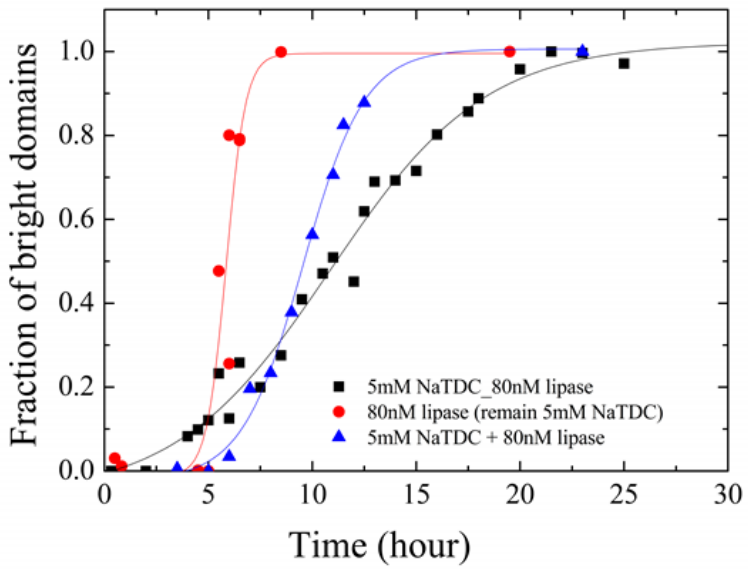

Figure 44: Fraction of bright domains at the LC/aqueous interface under a polarizing optical microscope for the hydrolysis of DPPC by 80 nM lipase. Before the addition of lipase, the DPPC-laden LC/aqueous interface had been incubated in 5mM NaTDC for 3 hours, and the NaTDC solution was then replaced by water.

To further study the role of NaTDC, we compared the lipolysis of the above three samples in the presence of colipase (Figure 45). Colipase was found to have two effects in lipolysis. One is that it can facilitate the adsorption of lipase to lipolysis products and bile salts [115]; another is that it can stabilize lipase in an open form [116]. By comparing Figure 44 to Figure 45, we find that the second sample has exactly the same trend with and without colipase (red circle in Figure 44 and Figure 45). This shows that colipase doesn't affect the sample when the sample has been incubated in NaTDC solution for a long time. So we infer the colipase actually plays the same role as NaTDC, therefore its effect becomes negligible when NaTDC fully exerts its functions. We infer that the promotion of the lipolysis by both

NaTDC and colipase is due to the stabilization of lipase in an open form. Because of this overlaid function of NaTDC and colipase, the effect of NaTDC in the lipolysis also diminishes in the presence of colipase, which is indicated by almost the same slope of the three samples in the burst phase in Figure 45. The lag time of these three samples in the presence of colipase is almost the same as in the absence of colipase. Since colipase has been known to facilitate the adsorption of lipase to bile salts at the interface [115, 117], the negligible effect of colipase again shows that the longer lag time is not due to the inhibition of NaTDC at the interface.

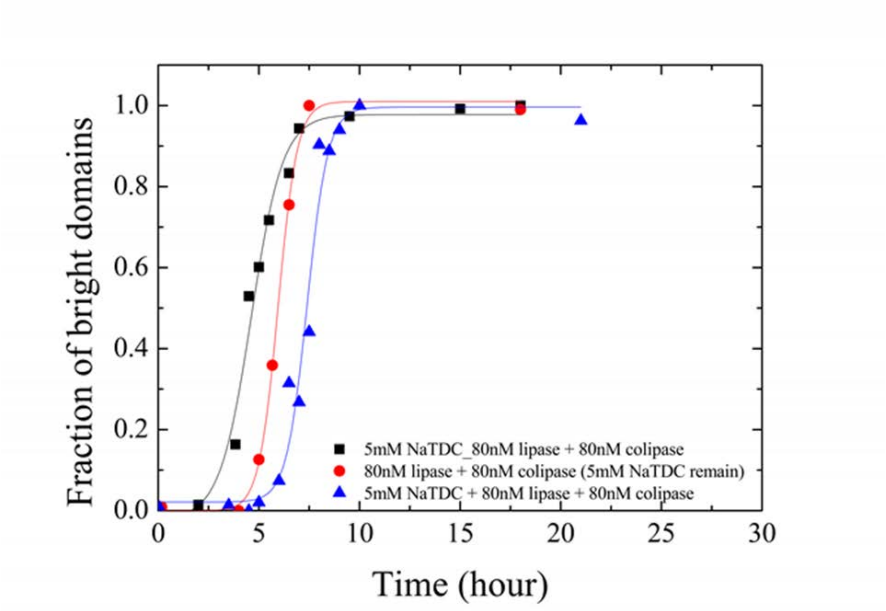

Figure 45: Fraction of bright domains at the LC/aqueous interface under polarizing optical microscope for the hydrolysis of DPPC by 80 nM lipase and 80 nM colipase. Before the addition of lipase, the DPPC-laden LC/aqueous interface has been incubated in 5mM NaTDC for 3 hours (black square, red circle), and the NaTDC solution was then replaced by water before the addition of lipase (black square), the 5mM NaTDC remains in the solution (red circle), and 5mM NaTDC added at the same time with lilpase (blue triangle).

5.3 Study of Other Factors on Lipolysis Processes Using LC-based Biosensors

The effect of temperature on the hydrolysis is also studied (Figure 46). The DPPC-laden LC/aqueous interface was made by immersing the LC film in 0.1mM DPPC solution for 1 hour, then replaced the DPPC solution by 5mM NaTDC solution. After the 3 hour incubation, the NaTDC solution was exchanged with deionized water. For 80 nM lipase without colipase, the lag time becomes longer and the hydrolysis process is faster at higher temperature. This can be explained by the increase of surface tension at higher temperature [118,

[119]. As the amount of DPPC is fixed at the interface, a higher temperature will lead to a higher surface tension. This will inhibit the penetration of lipase into the DPPC layer, so the lag time becomes longer. On the other hand, low surface tension can causes less denaturation of lipase at the lipid interface than high surface tension [119, 120]. Therefore, the activity of lipase is higher at low surface tension, which leads to the faster hydrolysis of DPPC. In the presence of colipase, colipase can help adsorption of lipase at the interface [115] and protect the denaturation of lipase [95] as well, so the difference between low and high temperature is less obvious.

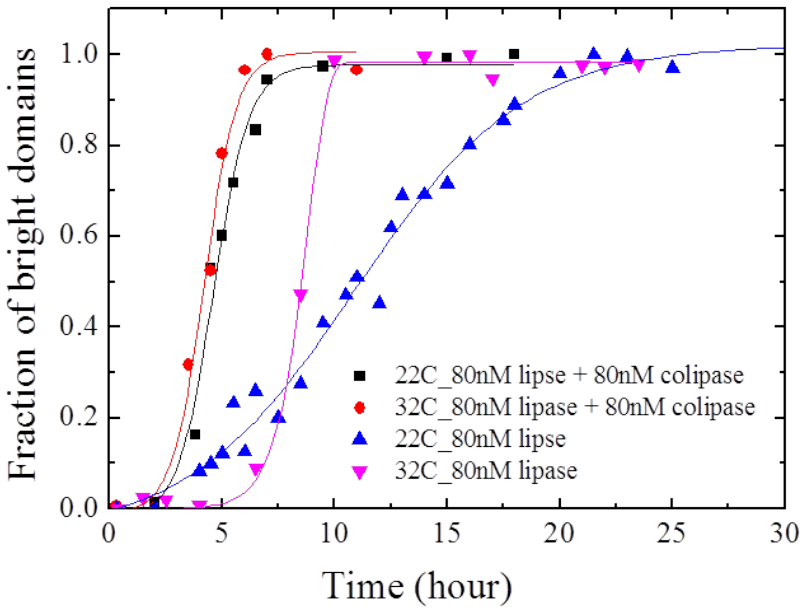

Figure 46: Hydrolysis of DPPC by 80 nM lipase in the presence (black square, red circle) and the absence (blue up triangle, magenta down triangle) of 80nM colipase at 22°C (black square, blue top triangle) and 32°C (red circle and blue down triangle).

The effect of calcium ions on hydrolysis is shown in Figure 47. The lag time is similar, but the hydrolysis with calcium ions is much faster. It is believed that calcium ions help to improve the activity of lipase [96, 117].

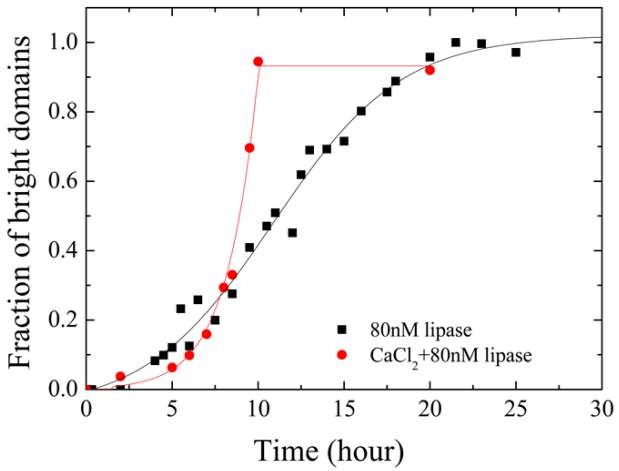

Figure 47: Slope of the transition area ratio versus time which reflects the hydrolysis speed for different concentrations of lipase and colipase.

The comparison between porcine pancreatic lipase (PPL) and phospholipase A_2 (PLA_2) has also been made (Figure 48). PLA_2 which specifically catalyzes the hydrolysis of phospholipases has shorter lag time and higher activity in either the presence of $CaCl_2$ or NaTDC. The slope of the burst phase of PPL is 4.8 times smaller than that of PLA_2. It was showed the activity of PPL against egg phosphatidylcholine is 1.27 times higher than PLA_2[106]. The difference lies in the difference of the substrate and the purity of lipases.

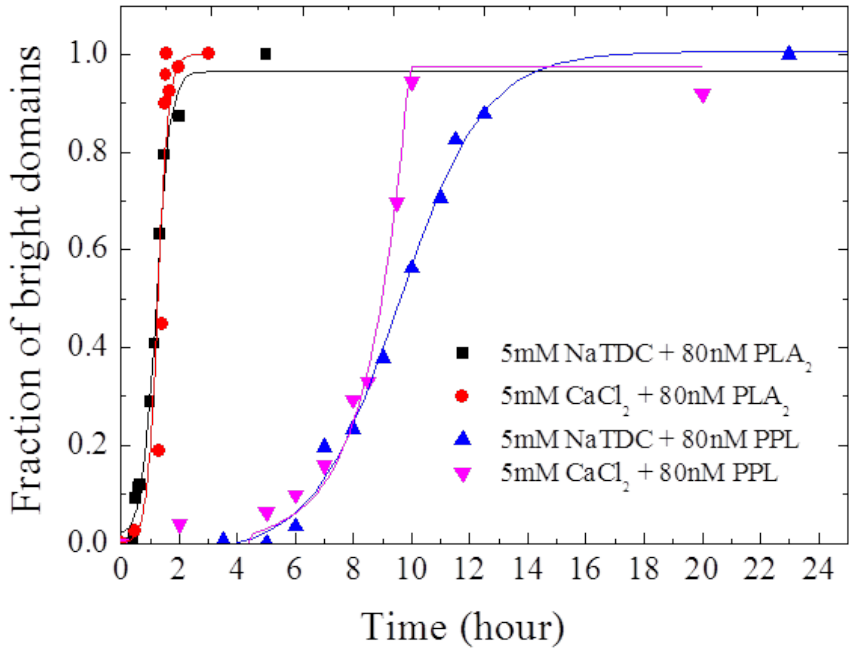

Figure 48: Comparison between the hydrolysis process by porcine pancreatic lipase (PPL) and the hydrolysis process by phospholipase A_2 (PLA_2) from porcine pancreas.

5.4 Conclusion

In this chapter, we have studied the effect of NaTDC on the hydrolysis of L-DPPC by the catalysis of PPL at the LC/aqueous interface through the observation of anchoring transition of the LC at the interface. We find that NaTDC at high concentrations can effectively disrupt the packing of the DPPC at the LC/aqueous interface, which enables the hydrolysis of DPPC by PPL. The NaTDC in the bulk solution prolongs the lag time of lipolysis, while the NaTDC at the interface can promote the lipolysis in the burst phase, which is probably due to the stabilization of PPL in the open form. We find that colipase and calcium ions also help with the hydrolysis.

The effect of temperature on the hydrolysis of the DPPC by PPL depends on the presence of colipase.

APPENDIX: LIST OF PUBLICATIONS

Journal Publications

[1] **S. He**, J. Deng, J. Fang, and S. T. Wu, “Lag-burst kinetics of surfactant displacement from the liquid crystal/aqueous interface by bile acids,” Colloids and Surfaces A, 471, 148-152 (2015)

[2] **S. He**, W. Liang, K.L. Cheng, J. Fang, and S.T. Wu, “Bile acid-surfactant interactions at the liquid crystal-aqueous interface,” Soft Matter, 10 (26), 4609 - 4614 (2014)

[3] W. Liang, **S. He**, J. Fang, “Self-Assembly of Light Harvesting Tubes for Sensitive and Selective Detection of Dopamine,” Langmuir, 30(3), 805-811 (2014)

[4] W. Liang, **S. He**, Y. Wang, J. Fang, “Morphology and shape control of porous silica nanostructures with dual-templating approaches,” J. Nanosci. Nanotechnol., 14(6), 4424-4430 (2014)

[5] S. He, W. Liang, K.L. Cheng, J. Fang, and S.T. Wu, “Liquid-crystal based sensors for the detection of cholic acid,” Anal. Methods, 5(16), 4126-4130 (2013).

[6] L. Rao, S. He, and S. T. Wu, "Blue-Phase Liquid Crystals for Reflective Projection Displays," J. Display Technology, 8(10), 555-557 (2012)

[7] S. He, J. H. Lee, H. C. Cheng, J. Yan, and S. T. Wu, “Fast-response blue-phase liquid crystal for color sequential displays,” J. Display Technology, 8(6), 352-356 (2012).

Conference Proceedings

[1] **S. He**, W. Liang, J. Fang, S. T. Wu, "Influence of chain lengths of liquid crystals on cholic acid detection," Proc. of SPIE, 8828, 88281G1-6 (2013).

[2] **S. He**, W. Liang, C. Tanner, J. Fang, S. T. Wu, "Liquid crystal based biosensors for bile acid detection," Proc. of SPIE, 8642, 86420P1-6 (2013).

[3] L. Rao, **S. He**, S. T. Wu, "Blue-Phase Liquid Crystals for Projection Displays," SID Symposium Digest of Technical Papers, 44, 902–904 (2013).

[4] **S. He**, J. H. Lee, J. Yan, H. C. Cheng, C. Y. Tsai, C. H. Lin, T. H. Huang, K. H. Liu, C. Y. Liu, N. Sugiura, W. L. Liau, and S. T. Wu, "Submillisecond-response blue-phase liquid crystal for color sequential projection displays," SID Symposium Digest of Technical Papers, 43, 918–921 (2012).

[5] H. Hu, D. A. Fishman, S. Webster, O. V. Przhonska, J. L. Bricks, A. D. Kachkovski, A. Terenziani, **S. He**, D. J. Hagan, and E. W. Van Stryland, "Two-photon Absorption Spectra of a Near-IR Polymethine Molecule with a Broken Ground-State Symmetry," OSA Technical Digest, FThW1 (2011).

REFERENCES

[1] Hofmann, A. F., and Mysels, K. J., Colloids and Surfaces, 30(1), 145-173 (1987).

[2] Thenard, L. J., Ann. Chim. (Paris), 64, 103-112 (1807).

[3] Hofmann, A. F., Arch Intern Med, 159(22), 2647-2658 (1999).

[4] Lefebvre, P., Cariou, B., Lien, F., Kuipers, F., and Staels, B., Physiol Rev, 89(1), 147-191 (2009).

[5] Hofmann, A. F., Archives of Internal Medicine, 159(22), 2647-2658 (1999).

[6] Lundeen, S. G., and Savage, D. C., Journal of Bacteriology, 172(8), 4171-4177 (1990).

[7] Alnouti, Y., Toxicol Sci, 108(2), 225-246 (2009).

[8] Bart Staels, V. A. F., DIABETES CARE 32, 32 (2) s237-s245 (2009).

[9] Wilde, P. J., and Chu, B. S., Adv Colloid Interface Sci, 165(1), 14-22 (2011).

[10] Patton, J. S., and Carey, M. C., Science, 204(4389), 145-148 (1979).

[11] Maldonado-Valderrama, J., Wilde, P., Macierzanka, A., and Mackie, A., Adv Colloid Interface Sci, 165(1), 36-46 (2011).

[12] Chu, B. S., Gunning, A. P., Rich, G. T., Ridout, M. J., Faulks, R. M., Wickham, M. S., Morris, V. J., and Wilde, P. J., Langmuir, 26(12), 9782-9793 (2010).

[13] Euston, S. R., Baird, W. G., Campbell, L., and Kuhns, M., Biomacromolecules, 14(6), 1850-1858 (2013).

[14] Westergaard, H., and Dietschy, J. M., Journal of Clinical Investigation, 58(1), 97-108 (1976).

[15] Denny Meyer, D. V. M., The European Journal of Comparative Gastroenterology, 3(1), 5-11 (1998).

[16] Dawson, P. A., Lan, T., and Rao, A., Journal of Lipid Research, 50(12), 2340-2357 (2009).

[17] Griffiths, W. J., and Sjovall, J., Journal of Lipid Research, (2009).

[18] Hong, Y. J., Turowski, M., Lin, J. T., and Yokoyama, W. H., J Agric Food Chem, 55(24), 9750-9757 (2007).

[19] Ye, L., Liu, S., Wang, M., Shao, Y., and Ding, M., J Chromatogr B Analyt Technol Biomed Life Sci, 860(1), 10-17 (2007).

[20] Horning, E. C., [Gas Phase Analytical Methods for the Study of Steroid Hormones and their Metabolites] Springer Berlin Heidelberg, 1 (1968).

[21] Wahlen, E., Tamasawa, N., Ichimiya, H., Egestad, B., and Sjovall, J., J Lipid Res, 35(10), 1902-1906 (1994).

[22] Persson, E., Lofgren, L., Hansson, G., Abrahamsson, B., Lennernas, H., and Nilsson, R., J Lipid Res, 48(1), 242-251 (2007).

[23] Sjövall, J., and Axelson, M., Journal of Pharmaceutical and Biomedical Analysis, 2(2), 265-280 (1984).

[24] Zhang, G. H., Cong, A. R., Xu, G. B., Li, C. B., Yang, R. F., and Xia, T. A., Biochem Biophys Res Commun, 326(1), 87-92 (2005).

[25] Kato, T., Yoneda, M., Nakamura, K., and Makino, I., Dig Dis Sci, 41(8), 1564-1570 (1996).

[26] Koide, S., Ito, N., and Karube, I., Biosensors and Bioelectronics, 22(9–10), 2079-2085 (2007).

[27] Liu, Y., Shi, J., and Guo, D. S., J Org Chem, 72(22), 8227-8234 (2007).

[28] Wu, Z., Hu, X., Tao, C.-a., Li, Y., Liu, J., Yang, C., Shen, D., and Li, G., Journal of Materials Chemistry, 18(45), 5452-5458 (2008).

[29] Scott J Woltman, G. D. J., Gregory P Crawford, [Liquid Crystals: Frontiers in Biomedical Applications] World Scientific Publishing Co., (2007).

[30] Drzaic, P. S., World Scientific, Singapore, (1995).

[31] Lockwood, N. A., Gupta, J. K., and Abbott, N. L., Surface Science Reports, 63(6), 255-293 (2008).

[32] Lavrentovich, O. D., Liq. Cryst. , 24, 117-125 (1998).

[33] Lansford, R., Bearman, G., and Fraser, S. E., J Biomed Opt, 6(3), 311-318 (2001).

[34] Ng, A. Y., See, C. W., and Somekh, M. G., J Microsc, 214(Pt 3), 334-340 (2004).

[35] Jakubiak, R., Natarajan, L. V., Tondiglia, V., He, G. S., Prasad, P. N., Bunning, T. J., and Vaia, R. A., Applied Physics Letters, 85(25), 6095-6097 (2004).

[36] Cheng, C.-C., Chang, C. A., and Yeh, J. A., Optics Express, 14(9), 4101-4106 (2006).

[37] Xu, S., Ren, H., and Wu, S.-T., Optics Express, 20(27), 28518-28523 (2012).

[38] Collings, P. J., Hird, M. , [Introduction to Liquid Crystals] Taylor & Francis Ltd., (1997).

[39] Clare, B. H., Guzman, O., de Pablo, J. J., and Abbott, N. L., Langmuir, 22(10), 4654-4659 (2006).

[40] Gupta, V. K., and Abbott, N. L., Physical Review E, 54(5), R4540-R4543 (1996).

[41] Jerome, B., Reports on Progress in Physics, 54(3), 391 (1991).

[42] Bai, Y., and Abbott, N. L., Langmuir, 27(10), 5719-5738 (2011).

[43] Faetti, S., and Marianelli, P., Phys Rev E Stat Nonlin Soft Matter Phys, 72(5 Pt 1), 051708 (2005).

[44] Bera, T., Liang, W., and Fang, J., Colloids and Surfaces A: Physicochemical and Engineering Aspects, 395(0), 32-37 (2012).

[45] Fang, J., Gehlert, U., Shashidar, R., and Knobler, C. M., Langmuir, 15(2), 297-299 (1999).

[46] Cheng, Y. L., Batchelder, D. N., Evans, S. D., Henderson, J. R., Lydon, J. E., and Ogier, S. D., Liquid Crystals, 27(10), 1267-1275 (2000).

[47] Gupta, J. K., Sivakumar, S., Caruso, F., and Abbott, N. L., Angew Chem Int Ed Engl, 48(9), 1652-1655 (2009).

[48] Gupta, J. K., Zimmerman, J. S., de Pablo, J. J., Caruso, F., and Abbott, N. L., Langmuir, 25(16), 9016-9024 (2009).

[49] Lin, I.-H., Miller, D. S., Bertics, P. J., Murphy, C. J., de Pablo, J. J., and Abbott, N. L., Science, 332(6035), 1297-1300 (2011).

[50] Brake, J. M., and Abbott, N. L., Langmuir, 18(16), 6101-6109 (2002).

[51] Gupta, J. K., Tjipto, E., Zelikin, A. N., Caruso, F., and Abbott, N. L., Langmuir, 24(10), 5534-5542 (2008).

[52] Brake, J. M., Daschner, M. K., Luk, Y.-Y., and Abbott, N. L., Science, 302(5653), 2094-2097 (2003).

[53] Tan, L. N., Bertics, P. J., and Abbott, N. L., Langmuir, 27(4), 1419-1429 (2010).

[54] Price, A. D., and Schwartz, D. K., Journal of the American Chemical Society, 130(26), 8188-8194 (2008).

[55] Hu, Q.-Z., and Jang, C.-H., Analyst, 137(3), 567-570 (2012).

[56] Oliver, J. F., Huh, C., and Mason, S. G., Journal of Colloid and Interface Science, 59(3), 568-581 (1977).

[57] Wu, S.-T., and Yang, D.-K., [Fundamentals of Liquid Crystal Devices] John Wiley & Sons Ltd, England(2006).

[58] Miller, D. S., Carlton, R. J., Mushenheim, P. C., and Abbott, N. L., Langmuir, 29(10), 3154-3169 (2013).

[59] Brake, J. M., Mezera, A. D., and Abbott, N. L., Langmuir, 19(16), 6436-6442 (2003).

[60] He, S., Liang, W., Tanner, C., Cheng, K.-L., Fang, J., and Wu, S.-T., Analytical Methods, 5(16), 4126-4130 (2013).

[61] Lockwood, N. A., and Abbott, N. L., Current Opinion in Colloid & Interface Science, 10(3–4), 111-120 (2005).

[62] Kawai, T., Kamio, H., Kondo, T., and Kon-No, K., The Journal of Physical Chemistry B, 109(10), 4497-4500 (2005).

[63] Chang, C.-H., and Franses, E. I., Colloids and Surfaces A: Physicochemical and Engineering Aspects, 100(0), 1-45 (1995).

[64] Leonard, M. R., Bogle, M. A., Carey, M. C., and Donovan, J. M., Biochemistry, 39(51), 16064-16074 (2000).

[65] Ho, Y. S., Porter, J. F., and McKay, G., Water, Air, and Soil Pollution, 141(1-4), 1-33 (2002).

[66] Plazinski, W., Rudzinski, W., and Plazinska, A., Advances in Colloid and Interface Science, 152(1–2), 2-13 (2009).

[67] Salahshoor, Z., and Shahbazi, A., European Journal of Environmental Sciences, 4(2), 116-130 (2014).

[68] He, S., Deng, J., Fang, J., and Wu, S.-T., Colloids and Surfaces A: Physicochemical and Engineering Aspects, 471(0), 148-152 (2015).

[69] He, S., Liang, W., Cheng, K.-L., Fang, J., and Wu, S.-T., Soft Matter, 10(26), 4609-4614 (2014).

[70] Armstrong, M. J., and Carey, M. C., J Lipid Res, 23(1), 70-80 (1982).

[71] Bera, T., and Fang, J., Langmuir, 29(1), 387-392 (2013).

[72] Cabral, D. J., Hamilton, J. A., and Small, D. M., J Lipid Res, 27(3), 334-343 (1986).

[73] Jana, P. K., and Moulik, S. P., The Journal of Physical Chemistry, 95(23), 9525-9532 (1991).

[74] Fini, A., and Roda, A., J Lipid Res, 28(7), 755-759 (1987).

[75] Carlton, R. J., Gupta, J. K., Swift, C. L., and Abbott, N. L., Langmuir, 28(1), 31-36 (2011).

[76] Bera, T., and Fang, J., Langmuir, 29(1), 387-392 (2012).

[77] Hakemi, H., Jagodzinski, E. F., and DuPre, D. B., The Journal of Chemical Physics, 78(3), 1513-1518 (1983).

[78] Alkhairalla, B., Allinson, H., Boden, N., Evans, S. D., and Henderson, J. R., Physical Review E, 59(3), 3033-3039 (1999).

[79] Chen, W., Martinez-Miranda, L. J., Hsiung, H., and Shen, Y. R., Physical Review Letters, 62(16), 1860-1863 (1989).

[80] Hiltrop, K., Hasse, J., and Stegemeyer, H., Berichte der Bunsengesellschaft für physikalische Chemie, 98(2), 209-213 (1994).

[81] Khoo, I. C. W., S. T., [Optics and Nonlinear Optics of Liquid Crystals] World Scientific Publishing Co. Ltd., (1993).

[82] Goodby, J. W., Liquid Crystals, 38(11-12), 1363-1387 (2011).

[83] Dąbrowski, R., Kula, P., and Herman, J., Crystals, 3(3), 443-482 (2013).

[84] Rezus, Y. L. A., and Bakker, H. J., Proceedings of the National Academy of Sciences, 103(49), 18417-18420 (2006).

[85] Somasundaran, P., [Encyclopedia of Surface and Colloid Science] CRC Press Inc, Boca Raton, FL(2006).

[86] Alme, B., Bremmelgaard, A., Sjovall, J., and Thomassen, P., J Lipid Res, 18(3), 339-362 (1977).

[87] Premasiri, W. R., Clarke, R. H., and Womble, M. E., Lasers in Surgery and Medicine, 28(4), 330-334 (2001).

[88] http://www.atsdr.cdc.gov/toxprofiles/tp115-c7.pdf, [Analytical methods for phenol].

[89] http://www.drugcheck.com/hc_uc-hs_urobilinogen.html, [Urobilinogen].

[90] Rachford, B. K., The Journal of Physiology, 12(1), 72-96 (1891).

[91] Willstatter, R., and Memmen, F., Hoppe-seyler's Z. Physiol. Chem. , 129, 1-25 (1923).

[92] Ye, P., Xu, Y.-J., Han, Z.-P., Hu, P.-C., Zhao, Z.-L., Lu, X.-L., and Ni, H.-G., Biochemical Engineering Journal, 80(0), 61-67 (2013).

[93] Knarreborg, A., Jensen, S. K., and Engberg, R. M., J Nutr Biochem, 14(5), 259-265 (2003).

[94] Gargouri, Y., Julien, R., Bois, A. G., Verger, R., and Sarda, L., J Lipid Res, 24(10), 1336-1342 (1983).

[95] Granon, S., and Semeriva, M., Eur J Biochem, 111(1), 117-124 (1980).

[96] Alvarez, F. J., and Stella, V. J., Pharm Res, 6(6), 449-457 (1989).

[97] Momsen, W. E., and Brockman, H. L., J Biol Chem, 251(2), 384-388 (1976).

[98] Wickham, M., Garrood, M., Leney, J., Wilson, P. D., and Fillery-Travis, A., J Lipid Res, 39(3), 623-632 (1998).

[99] Reis, P., Holmberg, K., Watzke, H., Leser, M. E., and Miller, R., Adv Colloid Interface Sci, 147-148, 237-250 (2009).

[100] Larsson, A., and Erlanson-Albertsson, C., Biochim Biophys Acta, 750(1), 171-177 (1983).

[101] Singh, J., and Ranganathan, R., The Journal of Physical Chemistry B, 118(8), 2077-2083 (2014).

[102] Grandbois, M., Clausen-Schaumann, H., and Gaub, H., Biophys J, 74(5), 2398-2404 (1998).

[103] Blank, M. L., and Snyder, F., Methods Enzymol, 197, 158-165 (1991).

[104] Okahata, Y., and Ebara, Y., Journal of the Chemical Society, Chemical Communications(2), 116-117 (1992).

[105] Gericke, A., and Hühnerfuss, H., Chemistry and Physics of Lipids, 74(2), 205-210 (1994).

[106] Aloulou, A., Frikha, F., Noiriel, A., Bou Ali, M., and Abousalham, A., Biochim Biophys Acta, 1841(4), 581-587 (2014).

[107] Brake, J. M., Daschner, M. K., and Abbott, N. L., Langmuir, 21(6), 2218-2228 (2005).

[108] Biltonen, R. L., and Lichtenberg, D., Chemistry and Physics of Lipids, 64(1–3), 129-142 (1993).

[109] Small, D. M., Penkett, S. A., and Chapman, D., Biochimica et Biophysica Acta (BBA) - Lipids and Lipid Metabolism, 176(1), 178-189 (1969).

[110] Gupta, J. K., Meli, M.-V., Teren, S., and Abbott, N. L., Physical Review Letters, 100(4), 048301 (2008).

[111] Wickham, M., Wilde, P., and Fillery-Travis, A., Biochim Biophys Acta, 1580(2-3), 110-122 (2002).

[112] Lairon, D., Charbonnier-Augeire, M., Nalbone, G., Leonardi, J., Hauton, J. C., Pieroni, G., Ferrato, F., and Verger, R., Biochim Biophys Acta, 618(1), 106-118 (1980).

[113] Borgström, B., Biochimica et Biophysica Acta (BBA) - Lipids and Lipid Metabolism, 488(3), 381-391 (1977).

[114] Miled, N., De Caro, A., De Caro, J., and Verger, R., Biochimica et Biophysica Acta (BBA) - Protein Structure and Molecular Enzymology, 1476(2), 165-172 (2000).

[115] Dahim, M., and Brockman, H., Biochemistry, 37(23), 8369-8377 (1998).

[116] Chu, B.-S., Gunning, A. P., Rich, G. T., Ridout, M. J., Faulks, R. M., Wickham, M. S. J., Morris, V. J., and Wilde, P. J., Langmuir, 26(12), 9782-9793 (2010).

[117] Brownlee, I. A., Forster, D. J., Wilcox, M. D., Dettmar, P. W., Seal, C. J., and Pearson, J. P., Nutr Res Rev, 23(1), 146-154 (2010).

[118] Sears, D. F., and Stark, R. E., [1 - Classic Techniques of Surface Science] Academic Press, (1973).

[119] Borgstrom, B., Biochim Biophys Acta, 712(3), 490-497 (1982).

[120] Rietsch, J., Pattus, F., Desnuelle, P., and Verger, R., J Biol Chem, 252(12), 4313-4318 (1977).